

# $N^*$ resonances from $K\Lambda$ amplitudes in sliced bins in energy

A.V. Anisovich<sup>1,2</sup>, V. Burkert<sup>3</sup>, M. Hadžimehmedović<sup>6</sup>, D.G. Ireland<sup>5</sup>, E. Klempt<sup>1,3</sup>, V.A. Nikonov<sup>1,2</sup>, R. Omerović<sup>6</sup>, A.V. Sarantsev<sup>1,2</sup>, J. Stahov<sup>6</sup>, A. Švarc<sup>4</sup>, and U. Thoma<sup>1</sup>

<sup>1</sup> Helmholtz-Institute für Strahlen- und Kernphysik der Universität Bonn, Nussallee 14 - 16, 53115 Bonn, Germany

<sup>2</sup> Particle and Nuclear Physics Institute, Orlova Rosha 1, 188300 Gatchina, Russia

<sup>3</sup> Thomas Jefferson Laboratory, 12000 Jefferson Avenue, Newport News, VA 23606, USA

<sup>4</sup> Rudjer Boskovic Institute, Bijenicka cesta 54, P.O. Box 180, 10002 Zagreb, Croatia

<sup>5</sup> SUPA, School of Physics and Astronomy, University of Glasgow, Glasgow G12 8QQ, United Kingdom

<sup>6</sup> University of Tuzla, Faculty of Natural Sciences and Mathematics, Univerzitetska 4, 75000 Tuzla, Bosnia and Herzegovina

Received: April 19, 2018/ Revised version:

**Abstract.** The two reactions  $\gamma p \rightarrow K^+ \Lambda$  and  $\pi^- p \rightarrow K^0 \Lambda$  are analyzed to determine the leading photoproduction multipoles and the pion-induced partial wave amplitudes in slices of the invariant mass. The multipoles and the partial-wave amplitudes are simultaneously fitted in a multichannel Laurent+Pietarinen model (L+P model), which determines the poles in the complex energy plane on the second Riemann sheet close to the physical axes. The results from the L+P fit are compared with the results of an energy-dependent fit based on the Bonn-Gatchina (BnGa) approach. The study confirms the existence of several poles due to nucleon resonances in the region at about 1.9 GeV with quantum numbers  $J^P = 1/2^+$ ,  $3/2^+$ ,  $1/2^-$ ,  $3/2^-$ ,  $5/2^-$ .

## 1 Introduction

The nucleon and its excited states are the simplest systems in which the non-abelian character of strong interactions is manifest. Three quarks is the minimum quark content of any baryon, and these three quarks carry the three fundamental colour charges of Quantum Chromodynamics (QCD), and combine to a colourless baryon. At present it is, however, impossible to calculate the spectrum of excited states from first principles, even though considerable progress in lattice gauge calculations has been achieved [1]. Models are therefore necessary when data are to be compared to predictions.

Quark models predict a rich excitation spectrum of the nucleon [2, 3, 4, 5, 6]. In quark models, the resonances are classified in shells according to the energy levels of the harmonic oscillator. The shell structure of the excitations is still seen in the data and reproduced in lattice calculations [1]. The first excitation shell is predicted to house five  $N^*$  and two  $\Delta^*$  resonances with negative-parity; all of them are firmly established. The second excitation shell contains *missing resonances*: 22 resonances (14  $N^*$ 's and 8  $\Delta^*$ 's) are predicted but 15 only are found in the mass range below 2100 MeV, and just 10 of them (5  $N^*$ 's and 5  $\Delta^*$ 's) are considered as established, with three or four stars in the notation of the Particle Data Group [7]. Thus 9  $N^*$ 's in the mass region between 1700 MeV and 2100 MeV are predicted to exist which are unobserved or the evidence for their existence is only fair or even poor. This deficit is known as the problem of the *missing resonances* [8, 9].

The search for missing resonances is one of the major aims of a number of experiments in which the interaction of a photon beam in the GeV energy range with a hydrogen and deuterium target is studied.

In  $\pi N$  elastic and charge exchange scattering, the excited states may have isospin  $I = 1/2$  ( $N^*$ ) and  $I = 3/2$  ( $\Delta^*$ ). A large amount of data was analyzed by the groups at Karlsruhe-Helsinki (KH84) [10], Carnegie-Mellon (CM) [11] and at GWU [12]. The 1850 - 2100 MeV mass region – where the missing resonances of the second excitation shell are predicted in most constituent quark models (see, e.g., [2, 3, 4, 5, 6, 13, 14]) – is dominated by the production of  $\Delta^*$  resonances with spin-parity  $J^P = 1/2^\pm, 3/2^\pm, 5/2^\pm, 7/2^+$ ; nucleon resonances are difficult to establish in this mass range due to the overwhelming background from  $\Delta^*$  resonances.

The production of  $\Lambda$  hyperons in pion and photo-induced reactions, in contrast to  $\pi N$  elastic scattering, is ideally suited to search for new nucleon resonances and to confirm resonances that are not yet well established (see, e.g., [13, 14] and references therein). Due to isospin conservation in strong interactions, only  $N^*$  resonances decay into  $\Lambda K$  final states, there are no isospin  $I = 3/2$  contributions. Second, the  $\Lambda \rightarrow N\pi$  weak-interaction decay reveals the polarization  $P$  of the  $\Lambda$ . Thus, the recoil polarization is measurable. In  $\pi N$  elastic scattering, the equivalent target polarization, also called  $P$ , requires the use of a polarized target. In photoproduction, a third advantage emerges: the process is not suppressed even when the  $\pi N$

coupling constants of  $N^*$  resonances in the second excitation shell are small [13,14]. Photoproduction may hence reveal the existence of  $N^*$  resonances coupling to  $\pi N$  only weakly. Indeed, a number of new resonances has been reported (or have been upgraded in the star rating) from a combined analysis of a large number of pion and photo-produced reactions [15]. Some of the “new” resonances had been observed before [10,11,16,17,18] or were confirmed in later analyses [19,20,21]. The evidence for the existence of the new states stemmed from energy-dependent fits to the data using the BnGa approach [22,23,24,25]. The reaction  $\gamma p \rightarrow K^+ \Lambda$  proved to be particularly useful [26].

The ultimate aim of experiments is to provide sufficient information that the data can be decomposed into partial waves or multipoles of defined and unique spin-parity. It can either be done through constructing an explicit theoretical model, or as we present here, through the reconstruction of partial-wave amplitudes and of multipoles in a truncated partial wave analysis. Limiting the partial wave series to low orbital angular momenta allows us to overcome issues with the still relatively large errors in the measurements of observable quantities.

The main goal of this paper is to test if  $N^*$  resonances in the fourth resonance region can be confirmed definitely from a fit to multipoles driving the excitation of partial waves with defined spin-parity, and to extract their properties. This is done in two ways: i.) In a standard way where a theoretical model is constructed. Its free parameters are estimated by fitting to the experimental data set base, and the partial waves of the final solution are analytically continued into the complex energy plane to obtain poles. ii.) In a way which does not depend on detailed model assumptions by using the Laurent+Pietarinen (L+P) method where a solution of the theoretical model is replaced by a most general analytic function consisting of a number poles and branch-cuts, which is embodied by a fast converging power series in a conformal variable. This variable is generated by a conformal mapping of the complex energy plane onto a unit circle. The first Riemann sheet is mapped to the outside of the unit circle, and the second Riemann sheet – where the poles are located – into the inside of the unit circle. In method ii.), poles are extracted by fitting to the single-energy partial wave decomposition, as opposed to a direct global fit to the data.

Method i.), coupled-channel energy-dependent fits, exploits the full statistical potential of the data. The effect of couplings to various other final states like  $N\pi$ ,  $N\eta$ ,  $\Sigma K$ ,  $\Delta\pi$ , etc. is taken into account exactly as well as all correlations between the different amplitudes. However, all partial waves need to be determined in one single fit, and it is difficult to verify the uniqueness of the results. In method ii.) we use single channel L+P fits (SC L+P) where each channel is fitted individually, and multi-channel L+P fits (MC L+P) where two or more channels are fitted simultaneously. The main advantage of the model-independent approach is that we can fit one partial wave at a time, and that we avoid any dependence on the quality of the model. The drawback is that you first have to extract par-

tial waves, and this procedure depends on the choice of higher partial waves, introducing some model dependence.

## 2 Construction of $K\Lambda$ amplitudes in slices of their invariant mass

### 2.1 The partial wave amplitudes for $\pi^- p \rightarrow K^0 \Lambda$

#### 2.1.1 Formalism

The differential cross sections  $d\sigma/d\Omega$  for the reaction  $\pi^- p \rightarrow K^0 \Lambda$  receives contributions from a spin-non-flip and a spin-flip amplitude,  $f$  and  $g$ , according to the relation

$$\frac{d\sigma}{d\Omega} = \frac{k}{q} (|f|^2 + |g|^2), \quad (1)$$

where  $q$  and  $k$  are the initial and final meson momenta respectively in the centre of mass frame [10]. Both amplitudes depend on the invariant mass  $W$  and  $z = \cos \theta$ , with  $\theta$  being the scattering angle. The two amplitudes can be expanded into partial wave amplitudes  $A_l^\pm$

$$f(W, z) = \frac{1}{\sqrt{qk}} \sum_{l=0}^L [(l+1)A_l^+(W) + lA_l^-(W)] P_l(z),$$

$$g(W, z) = \frac{1}{\sqrt{qk}} \sin \Theta \sum_{l=1}^L [A_l^+(W) - A_l^-(W)] P_l'(z), \quad (2)$$

where  $P_l(z)$  are the Legendre polynomials.  $J = |l \pm 1/2|$  is the total spin of the state. The sign in the relation for  $J$  defines the sign in  $A_l^\pm$ .

The  $\Lambda \rightarrow N\pi$  decay can be used to determine the decay asymmetry with respect to the scattering plane, called recoil asymmetry  $P$ . Assuming that the target nucleon is fully polarized,  $P$  can be defined as

$$(1 \pm P) \frac{d\sigma}{d\Omega} = |f \pm ig|^2. \quad (3)$$

When the target proton is polarized longitudinally (along the pion beam line), the spin transfer from proton to  $\Lambda$  yields the spin rotation angle  $\beta$ .

$$\beta = \arg \left( \frac{f - ig}{f + ig} \right) = \tan^{-1} \left( \frac{-2\Re(f^*g)}{|f|^2 - |g|^2} \right). \quad (4)$$

It is defined as  $\beta = \arctan(-R/A)$ , where  $A$  and  $R$  are the polarization components in direction of the  $\Lambda$  and its orthogonal component in the scattering plane.  $R$  and  $A$  are given by

$$R = \frac{2\Re(f^*g)}{|f|^2 + |g|^2}, \quad A = \frac{|f|^2 - |g|^2}{|f|^2 + |g|^2}. \quad (5)$$

The polarization variables are constrained by the relation

$$P^2 + A^2 + R^2 = 1. \quad (6)$$

### 2.1.2 Fits to the data

Data on the reaction  $\pi^- p \rightarrow K^0 \Lambda$  were taken in Chicago [27] and at the NIMROD accelerator at the Rutherford Laboratory [28, 29, 30]. From these data, the partial wave amplitudes  $A_l^\pm$  defined in eqn. (2) should be derived.

A detailed study showed that the data require angular momenta up to  $l = 3$  or even  $l = 4$  but do not have the precision to determine all partial wave amplitudes [31]. Therefore we try to determine at least the low- $l$  amplitudes, in particular  $A_1^- (= S_{11})$ ,  $A_0^+ (= P_{11})$ ,  $A_1^+ (= P_{13})$ , leading to  $J^P = 1/2^-, 1/2^+$ , and  $3/2^+$ . The higher partial waves, those above  $A_1^-$ ,  $A_0^+$ ,  $A_1^+$ , are taken from our current BnGa fit.

Figure 1 shows the data. The solid curves represent the final BnGa fit. It reproduces the data with a  $\chi^2/N_{\text{data}} = 570/916$ . The number of free parameters is 75.

The fit returns the real and imaginary parts of amplitudes for the  $S_{11}$ ,  $P_{11}$ , and  $P_{13}$  partial waves. The  $S_{11}$  and  $P_{11}$  amplitudes are shown in Fig. 2, the  $P_{13}$  amplitude in Ref. [31] only (since it could not be fit with the L+P method). The solid line represents the L+P fit described below, and the energy-dependent solution BnGa2011-02 is shown as error band. Note that the higher partial waves are constrained fixed to the BnGa solution, while the other lower amplitudes are free to adopt any values.

## 2.2 The multipoles for $\gamma p \rightarrow K^+ \Lambda$

### 2.2.1 Formalism

The amplitude for the reaction  $\gamma p \rightarrow K^+ \Lambda$  can be written in the form

$$A = \omega^* J_\mu \varepsilon_\mu \omega', \quad (7)$$

where  $\omega'$  and  $\omega$  are spinors representing the baryon in the initial and final state,  $J_\mu$  is the electromagnetic current of the nucleon, and  $\varepsilon_\mu$  characterizes the polarization of the photon. The amplitude can be expanded into four invariant (CGLN) amplitudes  $\mathcal{F}_i$  [32]

$$J_\mu = i\mathcal{F}_1 \sigma_\mu + \mathcal{F}_2 \frac{(\sigma \mathbf{q})}{|\mathbf{k}||\mathbf{q}|} \varepsilon_{\mu ij} \sigma_i k_j + i\mathcal{F}_3 \frac{(\sigma \mathbf{k})}{|\mathbf{k}||\mathbf{q}|} q_\mu + i\mathcal{F}_4 \frac{(\sigma \mathbf{q})}{q^2} q_\mu. \quad (8)$$

where  $\mathbf{q}$  is the momentum of the  $\Lambda$  hyperon in the final state,  $\mathbf{k}$  is the momentum of the nucleon in the initial state, calculated in the center-of-mass system of the reaction, and  $\sigma_i$  are the Pauli matrices. These four functions  $\mathcal{F}_i$  are functions of the invariant mass and of  $z$  with  $z = (\mathbf{k}\mathbf{q})/(|\mathbf{k}||\mathbf{q}|) = \cos \theta$  and  $\theta$  as the scattering angle. A determination of these four amplitudes requires the measurement with sufficient accuracy of at least eight well chosen observables [33, 34, 35, 36, 37]. For each slice in energy and angle one phase remains undetermined. It needs to be fixed from other sources. In  $\pi^\pm p$  elastic scattering, the phase can be determined from the (calculable) Coulomb interference. In hyperon production, one could try to fix

the phase to the phase of  $t$ -channel Kaon exchange. Once the  $\mathcal{F}_i$  functions are known for each energy and angle, the results of all experiments can be predicted.

The relations between the  $\mathcal{F}_i$  functions and the observables can be found, e.g., in [37]. For convenience, we give the expressions for the observables used in the fits. The differential cross section  $d\sigma/d\Omega$  and the single polarization observables, the beam asymmetry  $\Sigma$ , the recoil asymmetry  $P$ , and the target asymmetry  $T$ , are given by

$$\frac{d\sigma}{d\Omega} = \frac{k}{q} I = \frac{k}{q} \Re[\mathcal{F}_1 \mathcal{F}_1^* + \mathcal{F}_2 \mathcal{F}_2^* - 2z \mathcal{F}_2 \mathcal{F}_1^* + \quad (9a)$$

$$\frac{\sin^2(\theta)}{2} (\mathcal{F}_3 \mathcal{F}_3^* + \mathcal{F}_4 \mathcal{F}_4^* + 2\mathcal{F}_4 \mathcal{F}_1^* + 2\mathcal{F}_3 \mathcal{F}_2^* + 2z \mathcal{F}_4 \mathcal{F}_3^*)].$$

$$\Sigma I = -\frac{\sin^2(\theta)}{2} \times \quad (9b)$$

$$\Re[\mathcal{F}_3 \mathcal{F}_3^* + \mathcal{F}_4 \mathcal{F}_4^* + 2\mathcal{F}_4 \mathcal{F}_1^* + 2\mathcal{F}_3 \mathcal{F}_2^* + 2z \mathcal{F}_4 \mathcal{F}_3^*], \quad (9c)$$

$$P I = \sin(\theta) \Im m[(2\mathcal{F}_2^* + \mathcal{F}_3^* + z \mathcal{F}_4^*) \mathcal{F}_1 + \mathcal{F}_2^* (z \mathcal{F}_3 + \mathcal{F}_4) + \sin^2(\theta) \mathcal{F}_3^* \mathcal{F}_4], \quad (9d)$$

$$T I = \sin(\theta) \Im m[\mathcal{F}_1^* \mathcal{F}_3 - \mathcal{F}_2^* \mathcal{F}_4 + z(\mathcal{F}_1^* \mathcal{F}_4 - \mathcal{F}_2^* \mathcal{F}_3) - \sin^2(\theta) \mathcal{F}_3^* \mathcal{F}_4],$$

The double polarization observables  $O_{x'}$ ,  $O_{z'}$  ( $C_{x'}$ ,  $C_{z'}$ ) define the spin transfer from linearly (circularly) polarized photons to the  $\Lambda$  hyperon where the  $z'$  axis is given by the meson direction. This is referred to as the *primed* frame. Experimentally, the data on the spin transfer from polarized photons to the  $\Lambda$  hyperon are sometimes presented in an *unprimed* frame, in which the photon momentum is chosen as reference axis. Observables in the two frames are related by a simple rotation:

$$\begin{aligned} C_x &= \sin(\theta) C_{z'} + \cos(\theta) C_{x'}, \\ C_z &= \cos(\theta) C_{z'} - \sin(\theta) C_{x'}, \end{aligned}$$

with similar relations holding for the quantities  $O_{x'}$  and  $O_{z'}$ .

The double polarization observables  $O_{x'}$ ,  $O_{z'}$  ( $C_{x'}$ ,  $C_{z'}$ ) can be written as

$$O_{x'} I = \sin(\theta) \Im m[\mathcal{F}_2 \mathcal{F}_3^* - \mathcal{F}_1 \mathcal{F}_4^* + z(\mathcal{F}_2 \mathcal{F}_4^* - \mathcal{F}_1 \mathcal{F}_3^*)], \quad (9f)$$

$$O_{z'} I = -\sin^2(\theta) \Im m[\mathcal{F}_1 \mathcal{F}_3^* + \mathcal{F}_2 \mathcal{F}_4^*], \quad (9g)$$

$$C_{x'} I = \sin(\theta) \Re e[\mathcal{F}_2 \mathcal{F}_2^* - \mathcal{F}_1 \mathcal{F}_1^* + \mathcal{F}_2 \mathcal{F}_3^* - \mathcal{F}_1 \mathcal{F}_4^* + z(\mathcal{F}_2 \mathcal{F}_4^* - \mathcal{F}_1 \mathcal{F}_3^*)], \quad (9h)$$

$$C_{z'} I = \Re e[-2\mathcal{F}_1 \mathcal{F}_2^* + z(\mathcal{F}_1 \mathcal{F}_1^* + \mathcal{F}_2 \mathcal{F}_2^*) - \sin^2(\theta) (\mathcal{F}_1 \mathcal{F}_3^* + \mathcal{F}_2 \mathcal{F}_4^*)]. \quad (9i)$$

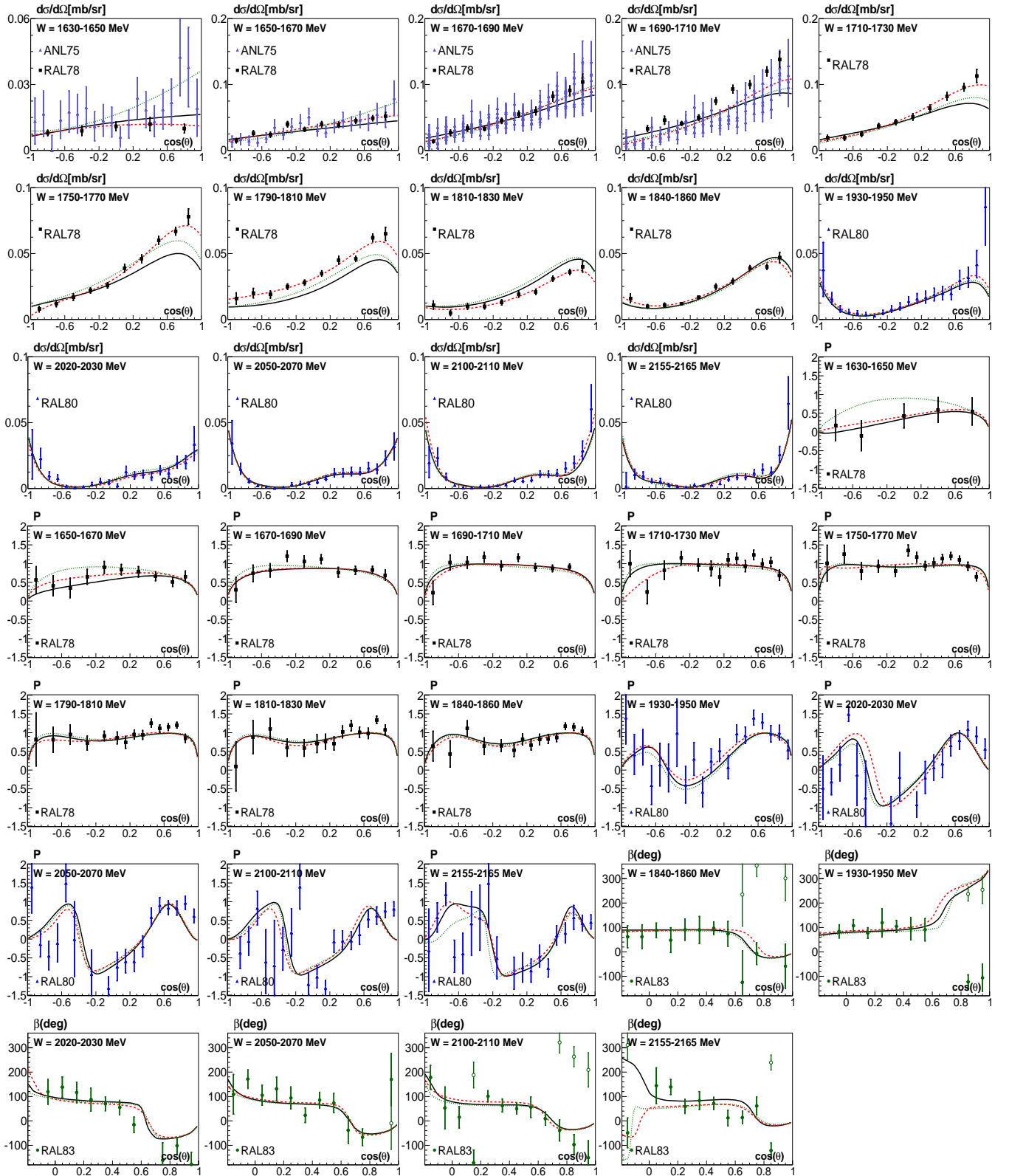


**Fig. 1.** Differential cross sections  $d\sigma/d\Omega$ ,  $\Lambda$  recoil polarization  $P$ , and spin rotation angle  $\beta$  for the reaction  $\pi^- p \rightarrow K^0 \Lambda$  from ANL75 (blue) [27] and RAL (black) [28,29,30]. Note that a few differential cross sections from [27] fall into a single energy window. The  $\beta$  is 360-degree cyclic which leads to additional data points shown by empty circles. The solid (black) line corresponds the  $L + P$  fit, the dashed (red) line corresponds the fit from which the amplitudes of Fig. 2 are deduced, the dotted (green) line corresponds to BnGa 2011-02 fit.

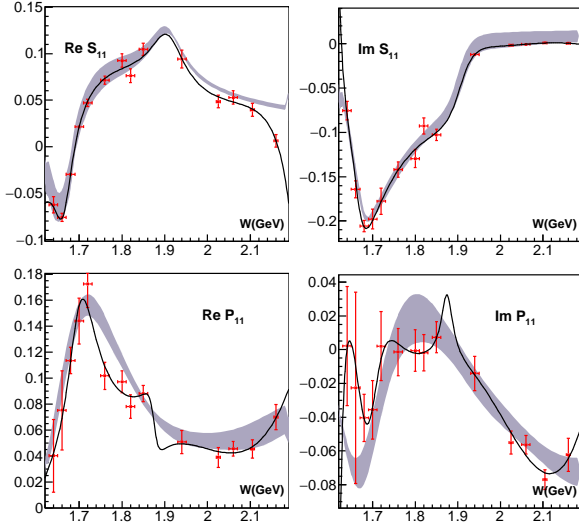


**Fig. 2.** Real and imaginary part of the (dimensionless)  $S_{11}$  and  $P_{11}$  waves [31]. The energy-dependent solution BnGa2011-02 is shown as error band. The band covers a variety of solutions when the model space was altered. The solid curve represents a L+P fit. The narrow structure in the  $P_{11}$  wave is enforced by the photoproduction data.

When the  $\mathcal{F}_i$  are known with sufficient statistical accuracy they can be expanded – for each slice in energy – into power series using Legendre polynomials  $P_L(z)$  and their derivatives:

$$\mathcal{F}_1(W, z) = \sum_{L=0}^{\infty} [LM_{L+} + E_{L+}] P'_{L+1}(z) + [(L+1)M_{L-} + E_{L-}] P'_{L-1}(z), \quad (10a)$$

$$\mathcal{F}_2(W, z) = \sum_{L=1}^{\infty} [(L+1)M_{L+} + LM_{L-}] P'_L(z), \quad (10b)$$

$$\mathcal{F}_3(W, z) = \sum_{L=1}^{\infty} [E_{L+} - M_{L+}] P''_{L+1}(z) + [E_{L-} + M_{L-}] P''_{L-1}(z), \quad (10c)$$

$$\mathcal{F}_4(W, z) = \sum_{L=2}^{\infty} [M_{L+} - E_{L+} - M_{L-} - E_{L-}] P''_L(z). \quad (10d)$$

Here,  $L$  corresponds to the orbital angular momentum in the  $K^+\Lambda$  system,  $W$  is the total energy,  $P_L(z)$  are Legendre polynomials with  $z$ , and  $E_{L\pm}$  and  $M_{L\pm}$  are electric and magnetic multipoles describing transitions to states with  $J = L \pm 1/2$ .  $M_{0+}$  or  $E_{1-}$  multipoles do not exist. Processes due to meson exchanges in the  $t$  channel may provide significant contributions to the reaction. They may demand high-order multipoles. The minimal  $L$  required to describe the data can be determined by polynomial expansions of the data [38]. A more direct approach is to

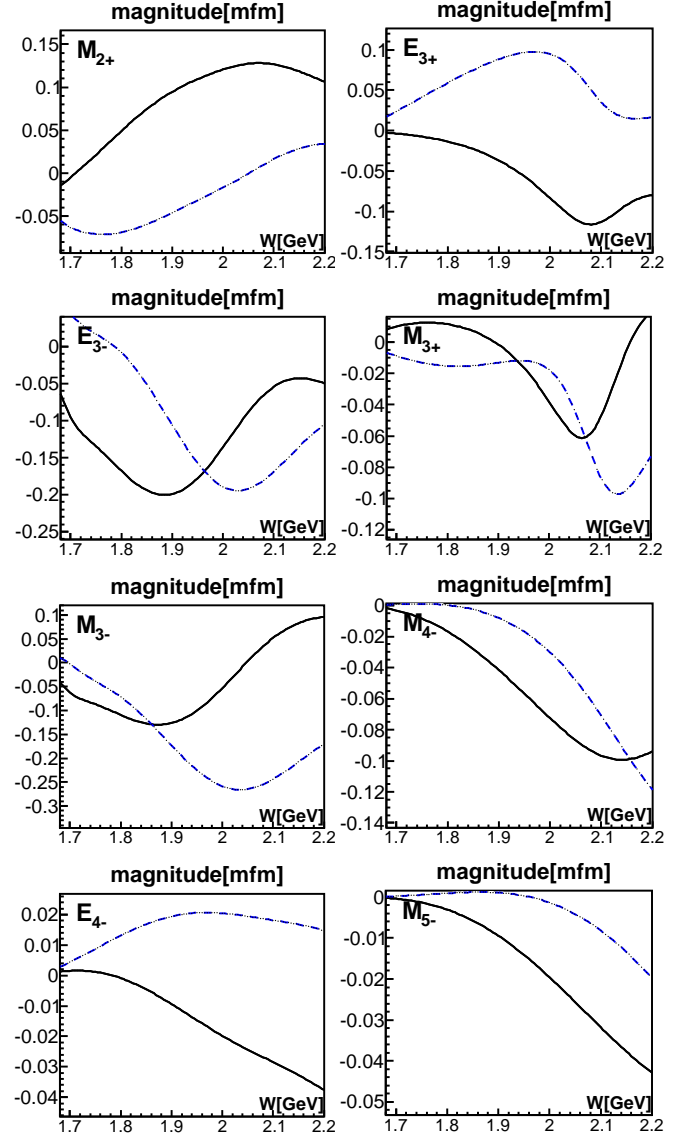


**Fig. 3.** (Color online) High- $L$  multipoles from BnGa fits to a large body of pion and photo-induced reactions. These multipoles are imposed in the fits to the data Figs. 4-7. Show real and imaginary part of  $M_{2+}$ ,  $M_{3-}$ ,  $E_{3-}$ ,  $M_{3+}$ ,  $E_{3+}$ ,  $M_{4-}$ ,  $E_{4-}$ ,  $M_{5-}$ . The solid (black) line is the real part of the multipole, dash (blue) line is the imaginary part of the multipole. The multipoles are given in mfm (milli-fermi=attometer).

insert the  $\mathcal{F}_i$  functions (eqns. 10) into the expressions for the observables (eqns. 9a and 9f) and to truncate the expansion at an appropriate value of  $L$  [39]. The observables are now functions of the invariant mass and the scattering angle, and the fit parameters are the electric and magnetic multipoles. In this method, the number of observables required to get the full information might be reduced if the number of contributing higher partial waves is not too big. But still, high precision is mandatory for the expansion.

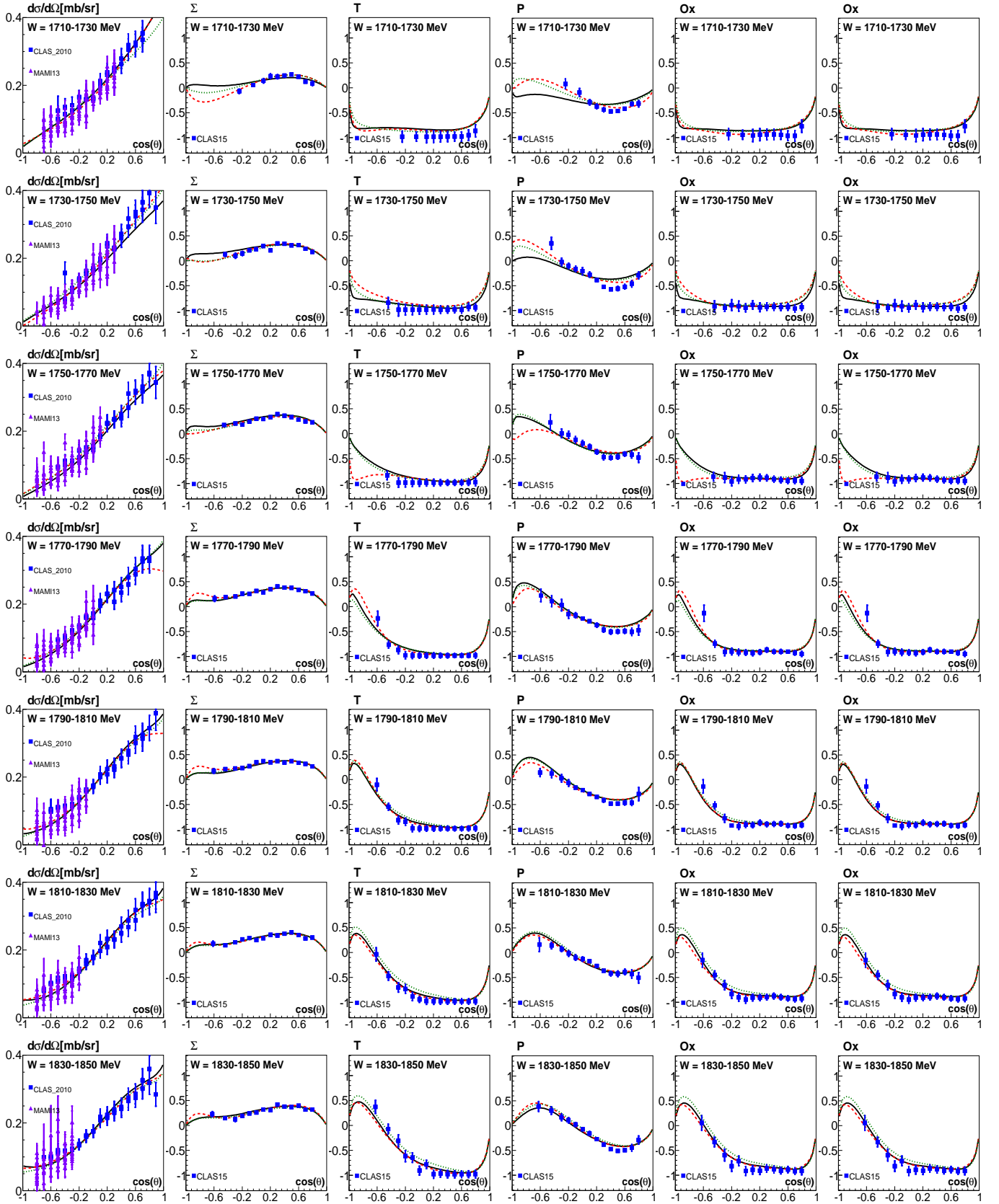


**Fig. 4.** (Color online) Fit to the data on  $d\sigma/d\Omega$ : [41],  $P$  [41], and  $\Sigma$ ,  $T$ ,  $O_x$ ,  $O_z$  [43] for  $\gamma p \rightarrow K^+ \Lambda$  reaction for the mass range from 1710 to 1850 MeV. The solid (black) line corresponds the  $L + P$  fit, the dashed (red) line corresponds to fit used to determine the multipoles of Fig. 8., the dotted (green) line corresponds to BnGa fit.

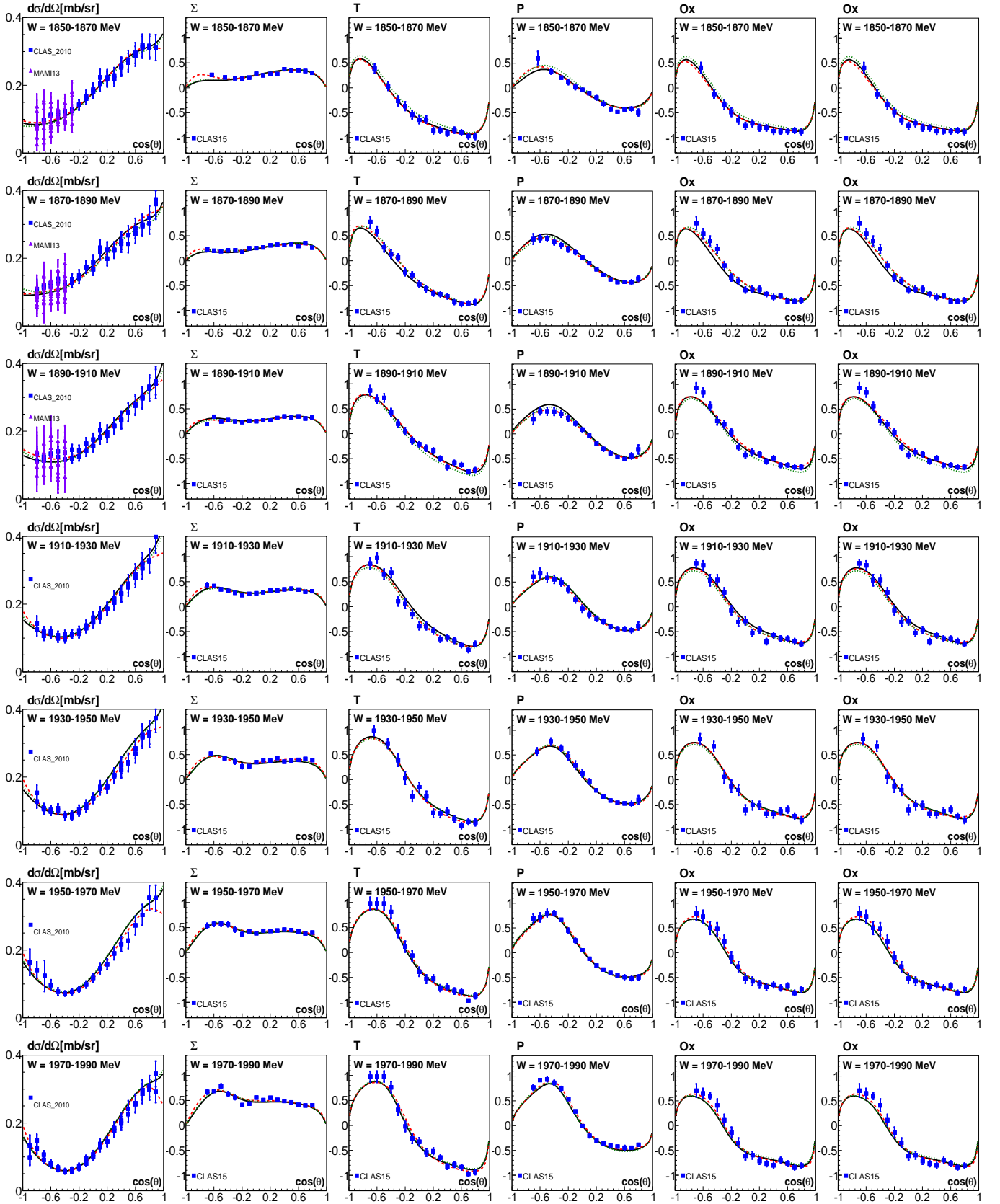


**Fig. 5.** (Color online) Fit to the data on  $d\sigma/d\Omega$ : [41],  $P$  [41], and  $\Sigma$ ,  $T$ ,  $O_x$ ,  $O_z$  [43] for  $\gamma p \rightarrow K^+ \Lambda$  reaction for the mass range from 1850 to 1990 MeV. The solid (black) line corresponds to the  $L + P$  fit, the dashed (red) line corresponds to fit used to determine the multipoles of Fig. 8., the dotted (green) line corresponds to BnGa fit.



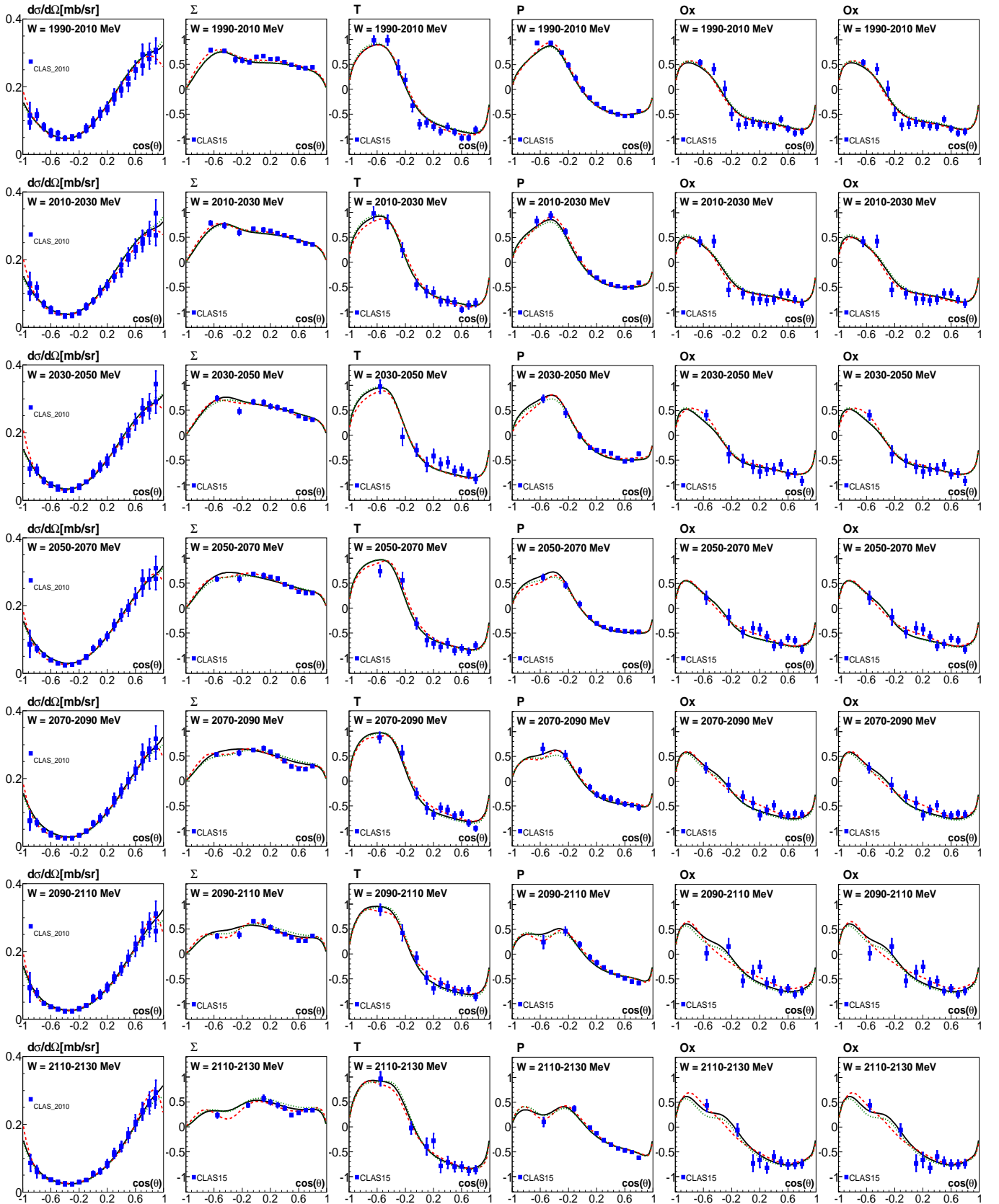


**Fig. 6.** (Color online) Fit to the data on  $d\sigma/d\Omega$ : [41],  $P$  [41], and  $\Sigma$ ,  $T$ ,  $O_x$ ,  $O_z$  [43] for  $\gamma p \rightarrow K^+ \Lambda$  reaction for the mass range from 1990 to 2130 MeV. The solid (black) line corresponds to the  $L + P$  fit, the dashed (red) line corresponds to fit used to determine the multipoles of Fig. 8., the dotted (green) line corresponds to BnGa fit.



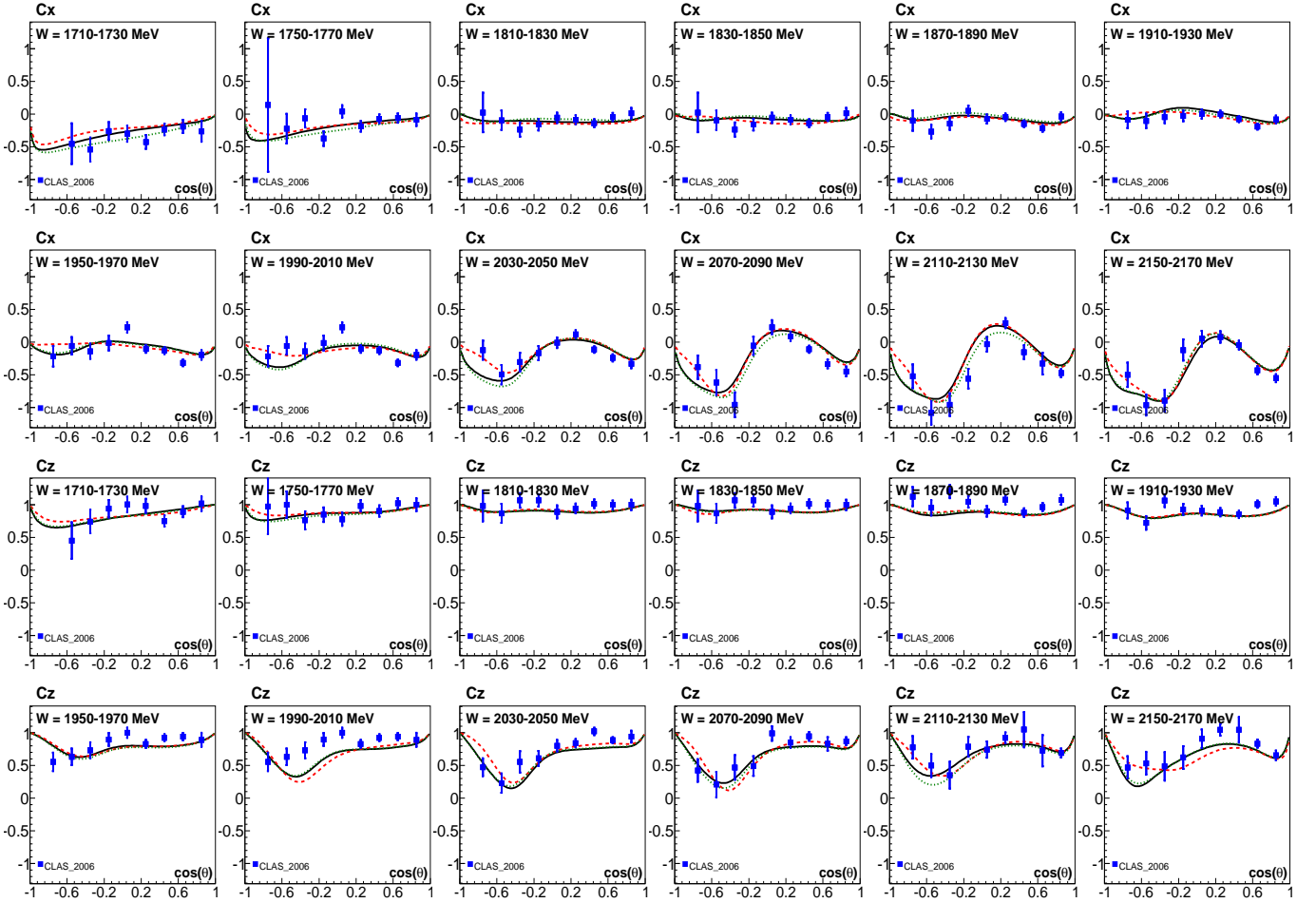


**Fig. 7.** (Color online) Fit to the data on  $C_x$  and  $C_z$  [42] for  $\gamma p \rightarrow K^+ \Lambda$  reaction. The solid (black) line corresponds the  $L + P$  fit, the dashed (red) line corresponds to fit used to determine the multipoles of Fig. 8., the dotted (green) line corresponds to BnGa fit.

### 2.2.2 Fits to the data

From the results of the BnGa analysis we expect that in the energy range considered here the  $E_{0+}$ ,  $M_{1-}$ , and  $E_{1+}$  yield the largest contributions, followed by  $M_{1+}$ ,  $E_{2-}$ , and  $M_{2-}$ . The  $E_{2+}$ ,  $M_{2+}$ ,  $M_{3-}$ ,  $E_{3-}$ ,  $M_{3+}$ ,  $E_{3+}$ ,  $M_{4-}$ ,  $E_{4-}$  all contribute with increasingly smaller importance, higher multipoles become negligible. First fits showed that it is not possible, given the statistical and systematic accuracy of the data, to determine all significant partial waves. Due to strong correlations between the parameters, the errors became large and the resulting multipoles showed large point-to-point fluctuations. Hence we decreased the number of freely fitted multipoles; the higher multipoles were fixed to the BnGa results. These multipoles are shown in Fig. 3. Reasonably small errors were obtained when the four multipoles  $E_{0+}$ ,  $M_{1-}$ ,  $E_{1+}$ , and  $M_{1+}$  were fitted. The errors increased only slightly when the multipoles  $E_{2-}$ ,  $M_{2-}$ , and  $E_{2+}$  were fitted in addition but constrained to the BnGa solution by a penalty function.

$$\chi_{pen}^2 = \sum_{\alpha} \frac{(M_{\alpha} - \hat{M}_{\alpha})^2}{(\delta \hat{M}_{\alpha})^2} + \sum_{\alpha} \frac{(E_{\alpha} - \hat{E}_{\alpha})^2}{(\delta \hat{E}_{\alpha})^2} \quad (11)$$

where  $\hat{E}_{\alpha}$  and  $\hat{M}_{\alpha}$  are the electric and magnetic multipoles from solution with  $E_{2-}$ ,  $M_{2-}$ , and  $E_{2+}$  fitted freely;  $\delta \hat{E}_{\alpha}$ ,  $\delta \hat{M}_{\alpha}$  are the multipole errors.

The reaction  $\gamma p \rightarrow K^+ \Lambda$  has been studied extensively by the CLAS collaboration. The early measurement of the differential cross sections  $d\sigma/d\Omega$  [40] was later superseded by a new measurement reporting the differential cross sections and the recoil polarization [41]. The spin transfer from circularly polarized photons to the final-state  $\Lambda$  hyperon, the quantities  $C_x$  and  $C_z$ , were reported in [42]. The polarization observables  $\Sigma$ ,  $T$ ,  $O_x$ ,  $O_z$  have been determined recently [43]. The data are shown in Figs. 4-6. The data are used to determine the photoproduction multipoles in a truncated partial wave analysis.

The final result for the multipoles are shown in Fig. 8. Strong variations are observed. The imaginary parts of all multipoles, except  $M_{2-}$  and  $E_{2+}$ , show threshold enhancements due to  $N(1650)1/2^-$  ( $E_{0+}$ ),  $N(1710)1/2^+$  ( $M_{1-}$ ),  $N(1720)3/2^+$  ( $E_{1+}$  and  $M_{1+}$ ),  $N(1700)3/2^-$  ( $E_{2-}$ ). Further structures are clearly seen at about 1900 MeV in the  $E_{0+}$ ,  $M_{1-}$ ,  $E_{1+}$ ,  $M_{1+}$ ,  $E_{2-}$ ,  $M_{2-}$  multipoles.

These structures emerge reliably when the multipole series is truncated, and only few multipoles are fitted freely. In Fig. 9 we show the results from one of our tests. In this case, the seven largest multipoles,  $E_{0+}$ ,  $M_{1-}$ ,  $E_{1+}$ ,  $M_{1+}$ ,  $E_{2-}$ ,  $M_{2-}$ , and  $E_{2+}$  were all left free. In several mass bins, the resulting multipoles show an erratic behavior; the results become unstable. Likewise, it was important to include the multipoles with large orbital angular momenta. Even though they are individually all small, neglecting them (by assuming that they are identically zero) leads to biased results. Furthermore, these multipoles fix the overall phase.

Sandorfi, Hoblit, Kamano, and Lee [37] have reconstructed the photoproduction amplitudes for the reaction  $\gamma p \rightarrow K^+ \Lambda$ . For the high partial waves, they used the Born amplitude. Partly, they fitted all waves with  $L \leq 3$  freely and determined the phases as differences to the  $E_{0+}$  phase. In other fits, they had the  $E_{0+}$  phase free and fitted all waves with  $L \leq 2$ . The resulting multipoles showed a wide spread. They concluded that a very significant increase in solid-angle coverage and statistics is required when all partial waves up to  $L = 3$  are to be determined.

### 3 BnGa fits to the data

The BnGa partial wave analysis uses a  $K$  matrix formalism to fit data on pion and photo-induced reactions to extract the leading singularities of the scattering or production processes. The formalism is described in detail in a series of publications [22, 23, 24, 25]. Here we briefly outline the dynamical part of the method.

The pion induced reaction  $\pi^- p \rightarrow K^0 \Lambda$  from the initial state  $i = \pi^- p$  to the final state  $j = K^0 \Lambda$  is described by a partial wave amplitude  $A_{ij}^{(\beta)}$ . It is given by a  $K$ -matrix which incorporates a summation of resonant and non-resonant terms in the form

$$A_{ij}^{(\beta)} = \sqrt{\rho_i} \sum_a K_{ia}^{(\beta)} \left( I - i\rho K^{(\beta)} \right)_{aj}^{-1} \sqrt{\rho_j}. \quad (12)$$

The multi-index  $\beta$  denotes the quantum numbers of the partial wave, it is suppressed in the following. The factor  $\rho$  represents the phase space matrix to all allowed intermediate states,  $\rho_i$ ,  $\rho_j$  are the phase space factors for the initial and the final state. The  $K$  matrix parametrizes resonances and background contributions:

$$K_{ab} = \sum_\alpha \frac{g_a^\alpha g_b^\alpha}{M_\alpha^2 - s} + f_{ab}. \quad (13)$$

Here  $g_{a,b}^\alpha$  are coupling constants of the pole  $\alpha$  to the initial and the final state. The background terms  $f_{ab}$  describe non-resonant transitions from the initial to the final state.

For photoproduction reactions, we use the helicity ( $h$ )-dependent amplitude for photoproduction  $a_b^h$  of the final state  $b$  [44]

$$a_b^h = P_a^h (I - i\rho K)_{ab}^{-1} \quad \text{where} \quad (14)$$

$$P_a^h = \sum_\alpha \frac{A_\alpha^h g_a^\alpha}{M_\alpha^2 - s} + F_a. \quad (15)$$

$A_\alpha^h$  is the photo-coupling of a pole  $\alpha$  and  $F_a$  a non-resonant transition. The helicity amplitudes  $A_\alpha^{1/2}$ ,  $A_\alpha^{3/2}$  are defined as residues of the helicity-dependent amplitude at the pole position and are complex numbers [45].

In most partial waves, a constant background term is sufficient to achieve a good fit. Only the background in the meson-baryon  $S$ -wave required a more complicated form:

$$f_{ab} = \frac{(a + b\sqrt{s})}{(s - s_0)}. \quad (16)$$

Further background contributions are obtained from the reggeized exchange of vector mesons [22] in the form

$$A = g(t)R(\xi, \nu, t) \quad \text{where} \quad (17)$$

$$R(\xi, \nu, t) = \frac{1 + \xi \exp(-i\pi\alpha(t))}{\sin(\pi\alpha(t))} \left( \frac{\nu}{\nu_0} \right)^{\alpha(t)}.$$

here,  $g(t) = g_0 \exp(-bt)$  represents a vertex function and a form factor.  $\alpha(t)$  describes the trajectory,  $\nu = \frac{1}{2}(s - u)$ ,  $\nu_0$  is a normalization factor, and  $\xi$  the signature of the trajectory. Pion and Pomeron exchange both have a positive signature and therefore [22]:

$$R(+, \nu, t) = \frac{e^{-i\frac{\pi}{2}\alpha(t)}}{\sin(\frac{\pi}{2}\alpha(t))} \left( \frac{\nu}{\nu_0} \right)^{\alpha(t)}. \quad (18)$$

Additional  $\Gamma$ -functions eliminate the poles at  $t < 0$ :

$$\sin\left(\frac{\pi}{2}\alpha(t)\right) \rightarrow \sin\left(\frac{\pi}{2}\alpha(t)\right) \Gamma\left(\frac{\alpha(t)}{2}\right). \quad (19)$$

where the Kaon trajectory is parametrized as  $\alpha(t) = -0.25 + 0.85t$ , with  $t$  given in  $\text{GeV}^2$ .

The data on partial wave amplitudes (Fig. 2) and on the photoproduction multipoles (Fig. 8) were included in the data base of the BnGa partial wave analysis. The data are fitted jointly with data on  $N\eta$ ,  $\Lambda K$ ,  $\Sigma K$ ,  $N\pi^0\pi^0$ , and  $N\pi^0\eta$  from both photo- and pion-induced reactions. Thus inelasticities in the meson-baryon system are constrained by real data. A list of the data used for the fit can be found in [15, 46, 47, 48] and on our website (pwa.hiskp.uni-bonn.de). In Fig. 2, the systematic errors define the error band; in Fig. 8, the systematic error of the real (imaginary) part of the amplitudes is shown a grey (red/blue) histogram at the bottom (top) line. The systematic errors are derived by a variation of the model space by adding further resonances with different spin-parities when the data are fitted.

## 4 The Laurent-Pietarinen expansion

### 4.1 Formalism

The main task of the single channel Laurent-Pietarinen expansion ( $SC_{L+P}$ ) is extracting pole positions from given partial waves for one reaction. The driving concept behind the method is to replace an elaborate theoretical

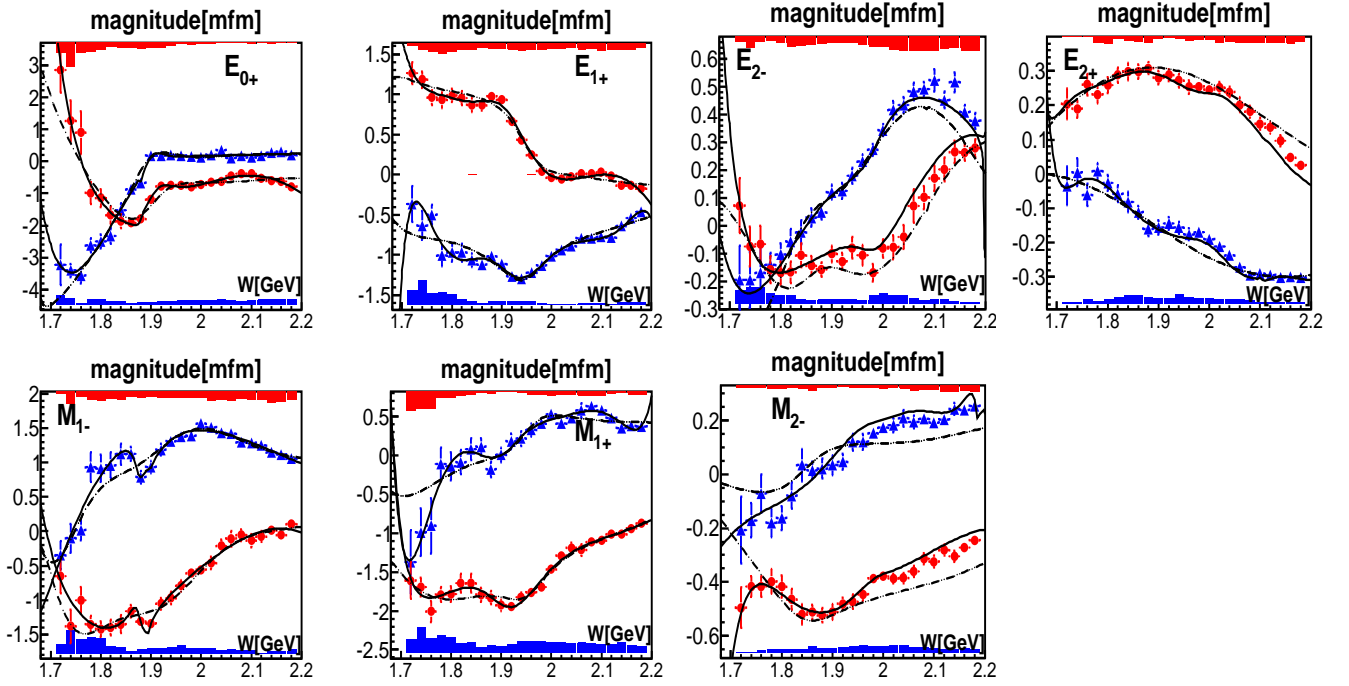


**Fig. 8.** (Color online) Real and imaginary parts of the multipoles derived from fits to the data shown in Figs. 4-6. The multipoles  $E_{0+}$ ,  $E_{1+}$ ,  $M_{1-}$ , and  $M_{1+}$  are fitted freely, the  $E_{2-}$ ,  $E_{2+}$ , and  $M_{2-}$  are forced by a penalty function to stay close to the BnGa fit. Higher-order multipoles are taken from the BnGa fit. The triangles (blue) mark the real part of the multipole, circles (red) mark the imaginary part of the multipole. Solid lines are L+P fits, dashed lines represent the BnGa fit. The grey (blue/red) areas denote the systematic errors derived from the spread when different BnGa solutions were used to determine the multipoles. The multipoles are given in mfm (milli-fermi=attometer).

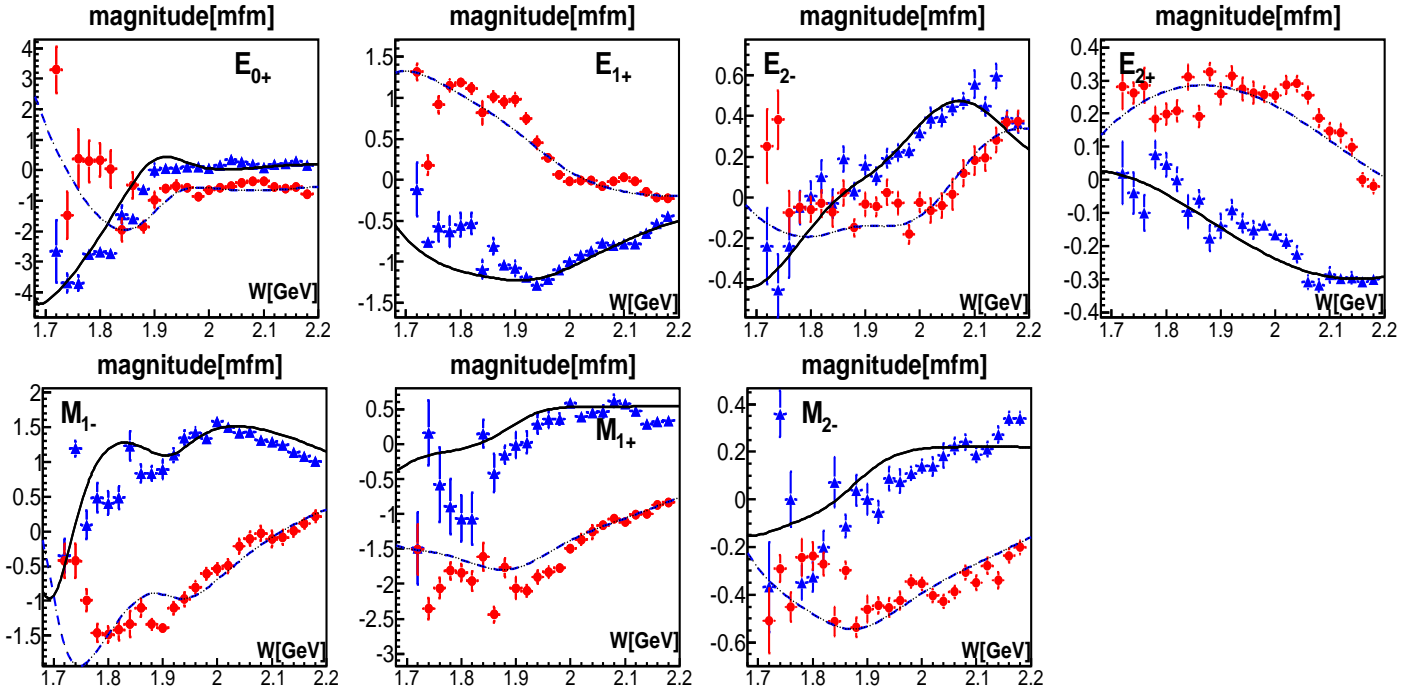


**Fig. 9.** (Color online) Real and imaginary parts of the  $E_{0+}$ ,  $E_{1+}$ ,  $M_{1-}$ ,  $M_{1+}$ ,  $E_{2-}$ ,  $E_{2+}$ , and  $M_{2-}$ . These multipoles were fitted freely. Higher-order multipoles are taken from the BnGa fit. The triangles (blue) mark the real part of the multipole, circles (red) mark the imaginary part of the multipole. Solid and dash lines represent the BnGa fit. The multipoles are given in mfm (milli-fermi=attometer).

model by a local power-series representation of partial wave amplitudes [49]. The complexity of a partial-wave analysis model is thus replaced by much simpler model-independent expansion which just exploits analyticity and unitarity. The L+P approach separates pole and regular part in the form of a Mittag-Leffler expansion<sup>1</sup>, and instead of modeling the regular part using some physical model it uses the conformal-mapping-generated, rapidly converging power series with well defined analytic properties called a Pietarinen expansion<sup>2</sup> to represent it effectively. So, the method replaces the regular part calculated in a model with the simplest analytic function which has correct analytic properties of the analyzed partial wave (multipole), and fits the given input. In such an approach the model dependence is minimized, and is reduced to the choice of the number and location of L+P branch-points used in the model. The method is applicable to both, theoretical and experimental input, and represents the first reliable procedure to extract pole positions directly from experimental data, with minimal model bias. The L+P expansion based on the Pietarinen expansion is used in some former papers in the analysis of pion-nucleon scattering data [51,52,53,54] and in several few-body reactions [21, 55,56]. The procedure has recently been generalized also to the multi-channel case [57].

The generalization of the L+P method to a multi-channel L+P method, used in this paper, is performed in the following way: i) separate Laurent expansions are made for each channel; ii) pole positions are fixed for all channels, iii) residua and Pietarinen coefficients are varied freely; iv) branch-points are chosen as for the single-channel model; v) the single-channel discrepancy function  $D_{dp}$  (see Eq. (5) in ref. [56]) which quantifies the deviation of the fitted function from the input is generalized to a multi-channel quantity  $D_{dp}^a$  by summing up all single-channel contributions, and vi) the minimization is performed for all channels in order to obtain the final solution.

The formulae used in the L+P approach are collected in Table 1.

L+P is a formalism which can be used for extracting poles from any given set of data, either theoretically generated, or produced directly from experiment. If the data set is theoretically generated, we can never reconstruct the analytical properties of the background put into the model, we can only give the simplest analytic function which on the real axes gives very similar, in practice indistinguishable result from the given model values. Therefore, analyzing partial waves coming directly from experiment is for L+P much more favourable because we do not have such demands. The analytic properties are unknown, so

there is no reason why the simplest perfect fit we offer should not be the true result. As in principle we do not care whether the input is generated by theory or otherwise, in the set of formulas given in Table 1. we denote any input fitted with L+P function  $T^a(W)$  generically as  $T^{a,exp}(W)$ .

In this paper we fit partial wave data; the discrete data points coming from a semi-constrained single energy fit of  $K\Lambda$  photo-production data, which is obtained in a way that the partial waves with  $L > 2$  are fixed to Bonn-Gatchina energy dependent partial waves, and lower ones are allowed to be free. We perform a multichannel fit ( $MC_{L+P}$ ) when possible by including single energy data from  $\pi N \rightarrow K\Lambda$  process, and we fit both multipoles for the same angular momentum at the same time in the coupled-multipole fit ( $CM_{L+P}$ ). The regular background part is represented by three Pietarinen expansion series, all free parameters are fitted. The first Pietarinen expansion with branch-point  $x_P$  is restricted to an unphysical energy range and represents all left-hand cut contributions. The next two Pietarinen expansions describe the background in the physical range with branch-points  $x_Q$  and  $x_R$  respecting the analytic properties of the analyzed partial wave. The second branch-point is mostly fixed to the elastic channel branch-point, the third one is either fixed to the dominant channel threshold, or left free. Thus, only rather general physical assumptions about the analytic properties are made like the number of poles and the number and the position of branch-points, and the simplest analytic function with a set of poles and branch-points is constructed.

In the compilation of our results we show the results of four fits: a) the BnGa coupled channel fit to the complete data base including the energy independent solutions for  $\pi^- p \rightarrow K^0 \Lambda$  and  $\gamma p \rightarrow K^+ \Lambda$  presented here; b) a single-channel L+P fit to the energy independent solution for  $\pi^- p \rightarrow K^0 \Lambda$  ( $SC_{L+P}^{\pi N, K\Lambda}$ ); c) a single-channel L+P fit to the energy independent solution for  $\gamma p \rightarrow K^+ \Lambda$  ( $SC_{L+P}^{\gamma N, K\Lambda}$ ); and d) a multi-channel L+P fit to the energy independent solution for  $\pi^- p \rightarrow K^0 \Lambda$  and  $\gamma p \rightarrow K^+ \Lambda$  ( $CC_{L+P}$ ).

## 4.2 L+P Fits

### 4.2.1 $J^P = 1/2^-$ -wave

We have fitted the  $J^P = 1/2^-$  partial wave from the energy independent amplitude for the reaction  $\pi^- p \rightarrow K^0 \Lambda$  in a  $SC_{L+P}^{\pi N, K\Lambda}$  fit. A  $\chi^2 = 2.45$  was obtained for the 28 data points with 23 parameters. We needed two poles, one at 1667 MeV and second one at 1910 MeV. Due to the low-statistics of the data, the results from the single-channel fit show large errors.

The 48 data points on the  $E_{0+}$  multipole from  $\gamma p \rightarrow K^+ \Lambda$  required only one pole close to 1900 MeV. The strong peak at low mass of the imaginary part of the  $E_{0+}$  multipole is reproduced by the function  $Y^a(W)$  with a branching point at the  $K^+ \Lambda$  threshold. Note that the lowest mass

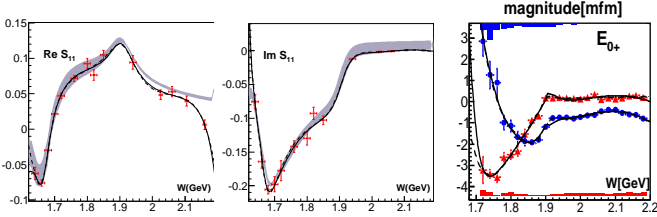
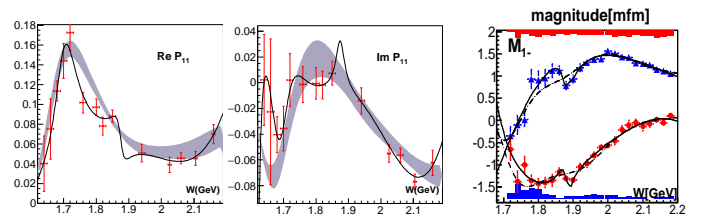
<sup>1</sup> Mittag-Leffler expansion [50] is the generalization of a Laurent expansion to a more-than-one pole situation. From now on, for simplicity, we will simply refer to this as a Laurent expansion.

<sup>2</sup> A conformal mapping expansion of this particular type was introduced by Ciulli and Fisher [51,52], was described in detail and used in pion-nucleon scattering by Esco Pietarinen [53,54], and named as a Pietarinen expansion by G. Höhler in [10].

**Table 1.** Formulae defining the Laurent+Pietarinen (L+P) expansion.

$$\begin{aligned}
T^a(W) &= \sum_{j=1}^{N_{pole}} \frac{x_j^a + i y_j^a}{W_j - W} + \sum_{k=0}^{K^a} c_k^a X^a(W)^k + \sum_{l=0}^{L^a} d_l^a Y^a(W)^l + \sum_{m=0}^{M^a} e_m^a Z^a(W)^m \\
X^a(W) &= \frac{\alpha^a - \sqrt{x_P^a - W}}{\alpha^a + \sqrt{x_P^a - W}}; \quad Y^a(W) = \frac{\beta^a - \sqrt{x_Q^a - W}}{\beta^a + \sqrt{x_Q^a - W}}; \quad Z^a(W) = \frac{\gamma^a - \sqrt{x_R^a - W}}{\gamma^a + \sqrt{x_R^a - W}} \\
D_{dp}^a &= \frac{1}{2 N_W^a - N_{par}^a} \sum_{i=1}^{N_W^a} \left\{ \left[ \frac{\Re T^a(W^{(i)}) - \Re T^{a,exp}(W^{(i)})}{Err_{i,a}^{\Re}} \right]^2 + \left[ \frac{\Im T^a(W^{(i)}) - \Im T^{a,exp}(W^{(i)})}{Err_{i,a}^{\Im}} \right]^2 \right\} + \mathcal{P}^a \\
\mathcal{P}^a &= \lambda_c^a \sum_{k=1}^{K^a} (c_k^a)^2 k^3 + \lambda_d^a \sum_{l=1}^{L^a} (d_l^a)^2 l^3 + \lambda_e^a \sum_{m=1}^{M^a} (e_m^a)^2 m^3 \quad D_{dp} = \sum_a^{all} D_{dp}^a
\end{aligned}$$

$a$  ..... channel index  $N_{pole}$  ..... number of poles  $W_j, W \in \mathbb{C}$   
 $x_i^a, y_i^a, c_k^a, d_l^a, e_m^a, \alpha^a, \beta^a, \gamma^a \dots \in \mathbb{R}$   
 $K^a, L^a, M^a \dots \in \mathbb{N}$  number of Pietarinen coefficients in channel  $a$ .  
 $D_{dp}^a$  ..... discrepancy function in channel  $a$   $N_W^a$  ..... number of energies in channel  $a$   
 $N_{par}^a$  ..... number of fitting parameters in channel  $a$   $\mathcal{P}^a$  ..... Pietarinen penalty function  
 $\lambda_c^a, \lambda_d^a, \lambda_e^a$  ..... Pietarinen weighting factors  $x_P^a, x_Q^a, x_R^a \in \mathbb{R}$  (or  $\in \mathbb{C}$ ).  
 $Err_{i,a}^{\Re, \Im}$  ..... minimization error of real and imaginary part respectively.

**Fig. 10.** (Color online) Real and imaginary parts of the  $J^P = 1/2^-$ :  $S_{11}$  partial wave amplitude, and the  $E_{0+}$  multipole. The grey band represents the allowed range of BnGa solutions, the dashed curve the single channel fits  $SC_{L+P}^{\pi N, K\Lambda}$  and  $SC_{L+P}^{\gamma N, K\Lambda}$ , and the solid curves the L+P fit to both data sets.**Fig. 11.** (Color online) Real and imaginary parts of the  $J^P = 1/2^+$ :  $P_{11}$  partial wave amplitude, and the  $M_{1-}$  multipole. The grey band represents the allowed range of BnGa solutions, the dashed curve the single channel fits  $SC_{L+P}^{\pi N, K\Lambda}$  and  $SC_{L+P}^{\gamma N, K\Lambda}$ , and the solid curves the L+P fit to both data sets.

bin for the  $E_{0+}$  multipole starts at 1700 MeV, significantly above the  $N(1650)1/2^-$  mass. The data were described with a  $\chi^2 = 0.48$  and 19 parameters in a  $SC_{L+P}^{\gamma N, K\Lambda}$  fit. Compared to the pion-induced reaction, the errors on the higher-mass resonance (at 1900 MeV) are considerably reduced.

The common fit to both data sets (with 76 data points) used two poles, the fit resulted in a  $\chi^2 = 0.86$  for 37 parameters. The results are shown in Table 2 and Figs. 8 and 10.

The real part of the pole positions of the  $N(1650)1/2^-$  resonance are nicely consistent when the three values are compared, the imaginary part is likely too narrow in the L+P fit. The magnitudes of the inelastic pole residue are consistent at the  $2\sigma$  level when the BnGa and CC L+P fits are compared. The phases, however, seem to be inconsistent.

The  $N(1895)1/2^-$  pole positions are well defined with acceptable errors and consistent when the four analyses are compared, only the single-channel L+P fit to photo-

production data returns a slightly too narrow width. All four analyses yield compatible magnitudes of the inelastic pole residues, the phases disagree at the  $2\sigma$  level. The magnitudes and the phases of the  $E_{0+}$  multipole determined by the BnGa fit agree well with the values of the L+P fit within the rather large uncertainties. Note that the errors in the CC L+P and BnGa fits have different origins: The L+P errors are of a statistical nature, the BnGa errors are derived from the spread of results of a variety of different fits. Both approaches establish the need for  $N(1650)1/2^-$  and unquestionably require  $N(1895)1/2^-$ .

#### 4.2.2 $J^P = 1/2^+$ -wave

We have fitted the  $J^P = 1/2^+$ -wave using the  $P_{11}$  energy independent amplitude for the  $\pi^- p \rightarrow K^0 \Lambda$  reaction and the  $M_{1-}$  multipole from  $\gamma p \rightarrow K^+ \Lambda$ . The first data set  $\pi^- p \rightarrow K^0 \Lambda$  required two poles. The first pole was located near 1700 MeV, the second one was found near 2100 MeV

even though with large error bars: the admitted range covers masses from  $\sim 1790$  to  $\sim 2375$  MeV. The photoproduction data required only one pole close to 1900 MeV. The CC L+P fit to both data sets was performed with two poles.

The results are shown in Table 2 and Figs. 8 and 11. The 28 data points for  $\pi^-p \rightarrow K^0\Lambda$  were fitted with 23 parameters and a  $\chi^2 = 0.67$ . The 48 data points on the  $M_{1-}$  multipole were described with a  $\chi^2 = 0.366$  and 19 parameters. The common fit to both data sets resulted in a  $\chi^2 = 0.505$  for 41 parameter. Both approaches, the BnGa and CC L+P fit, establish the need for  $N(1710)1/2^+$ , and unquestionably require  $N(1880)1/2^+$ .

The  $N(1710)1/2^+$  mass is consistent in the CC L+P and the BnGa fits, its width tends to be smaller in the CC L+P fit, see Tables 2 but the difference is  $1.7\sigma$  only. The magnitudes of the inelastic residue for this resonance have large error bars in the L+P fits and cover zero, we give upper limits only. The limits are compatible with the BnGa result. In spite of the large errors in the magnitudes, the phases are consistent.

The masses of the  $N(1880)1/2^+$  resonance from the BnGa and CC L+P fits are compatible but not the widths. The inelastic residues disagree slightly. Both, the single-channel SC L+P and the coupled-channel CC L+P fit, agree that the  $N(1880)1/2^+$  width should be smaller than  $\sim 40$  MeV while BnGa finds a normal hadronic width. However, we have performed a CC L+P fit imposing a mass of 150 MeV. When the result of the CC L+P fit is compared to the observables with 674 data points (Figs. 4 to 7), the fit deteriorates only minimally, the  $\chi^2$  increases by 4.5 units. We conclude that the  $N(1880)1/2^+$  resonance is definitely required in this nearly model-independent analysis and that it has a normal hadronic width. The magnitudes of the inelastic residues and of the  $M_{1-}$  multipole agree reasonably well, the phases of the inelastic residues are again inconsistent while the  $M_{1-}$  multipole phases agree well within their uncertainties.

#### 4.2.3 $J^P = 3/2^+$ -wave

The  $J^P = 3/2^+$ -wave was not derived from the pion induced reaction  $\pi^-p \rightarrow K^0\Lambda$ , so the two photoproduction multipoles  $E_{2-}$  and  $M_{2-}$  were fitted simultaneously in the coupled-multipoles L+P mode ( $\text{CM}_{\text{L+P}}$ ). The CM L+P fit required only one pole close to 1900 MeV, no  $N(1720)3/2^+$  was needed. Due to the presence of important thresholds ( $\Sigma K$ ,  $N(1520)3/2^-\pi$ ,  $N(1535)1/2^-\pi$ ), the  $N(1720)3/2^+$  resonance has a rather complicated pole structure, and we refrain from discussing this resonance here. The fit to the 96 data points in the two data sets is shown in Fig. 8. The fit returned a  $\chi^2 = 0.42$  for 35 parameters. The results are shown in Table 3. The poles from the L+P and BnGa fits are fully consistent. We conclude that  $N(1900)3/2^+$  is definitely confirmed in this nearly model-independent analysis.

#### 4.2.4 $J^P = 3/2^-$

Due to limited statistics, the  $J^P = 3/2^-$ -wave could not be derived from the pion induced reaction  $\pi^-p \rightarrow K^0\Lambda$ . Thus, only the two photoproduction multipoles  $E_{1+}$  and  $M_{1+}$  were fitted in the coupled-multipoles CM L+P mode ( $\text{CM}_{\text{L+P}}$ ). The L+P fit to the 96 data points in the two data sets returned a  $\chi^2 = 0.55$  for 36 parameters, the fit is shown in Fig. 8. The fit required only one pole close to 1900 MeV, no  $N(1700)3/2^-$  was needed. A low-mass pole at about 1700 MeV is required in the BnGa fit but due to the complicated pole structure in this mass region, we again refrain from discussing its properties here. The results of the L+P and the BnGa fits are shown in Table 3. The poles from the L+P and BnGa fits are found to be inconsistent. In the BnGa model, a mass of  $1870 \pm 25$  MeV is found, and there is a second pole – not discussed here – at 2150 MeV. The L+P fit does not find evidence for a two-pole structure and places the mass of the one pole at  $1977 \pm 41$  MeV.

#### 4.2.5 $J^P = 5/2^-$ -waves

The  $J^P = 5/2^-$ -wave was not derived from the pion induced reaction  $\pi^-p \rightarrow K^0\Lambda$ , and in this case only the  $E_{2-}$  multipole could be determined from the data. The single channel L+P mode ( $\text{SC}_{\text{L+P}}^{\gamma N, K\Lambda}$ ) was hence used to fit the data. The fit required one pole at about 2000 MeV. The fit to the 48 data points in the two data sets returned a  $\chi^2 = 0.60$  for 25 parameters. The results are shown in Table 3 and Fig. 8. The pole positions from the L+P and BnGa fits are fully consistent. We conclude that  $N(2060)5/2^-$  is confirmed.

## 5 Comparison to other groups

Figure 12 shows the real and imaginary parts of low- $L$  partial-wave amplitudes from Refs. [31] and [58]. The amplitudes are similar in magnitude but differ in their shape. The JüBo fit does not contain  $N(1895)1/2^-$ , the third resonance in the  $J^P = 1/2^-$  wave that is confirmed here and in a recent analysis of  $\gamma p \rightarrow \eta, \eta'p$  [59]. Both the analysis in Ref. [58] and this work, introduce  $N(1710)1/2^+$  - a resonance not needed in Ref. [12] - but here we find evidence for an additional resonance in this partial wave,  $N(1880)1/2^+$ . Thus the differences in the partial-wave amplitudes are to be expected.

There is a large number of papers devoted to partial wave analyses of the reaction  $\gamma p \rightarrow K^+\Lambda$ . We discuss here only recently published papers which include at least one measurement of a double polarization variable.

The Gent group proposes a methodology based on Bayesian inference to determine those resonances which contribute to  $\gamma p \rightarrow K^+\Lambda$  [60, 61]. They try different groups of 11 resonances and find that the fit with  $N(1535)1/2^-$ ,  $N(1650)1/2^-$ ,  $N(1680)5/2^+$ ,  $N(1720)3/2^+$ ,  $N(1875)3/2^-$ ,  $N(1880)1/2^+$ ,  $N(1900)3/2^+$ , and  $N(2000)5/2^+$  has the highest evidence.

**Table 2.** Pole parameters for the  $J^P = 1/2^-$  and  $1/2^+$  waves from the BnGa multichannel partial-wave analysis (BnGa), from the single channel L+P fits to fits to  $\pi N \rightarrow K\Lambda$  and  $\gamma p \rightarrow K^+\Lambda$  (SC), and from the combined L+P fit to  $\gamma p \rightarrow K^+\Lambda$  and  $\pi^- p \rightarrow K^0\Lambda$  (CC). Masses and widths are given in MeV. The acronym  $|a_1(\pi N \rightarrow K\Lambda)|$  stands for the normalized residua  $2|Res_1(\pi N \rightarrow K\Lambda)|/\Gamma_{\text{pole}}$ ,  $|A_1(E_{0+})|$  for the residua  $|Res_1(E_{0+}(\gamma N \rightarrow K\Lambda))|$ ; they are given in  $\text{GeV}^{-1/2}$ . The phases  $\Theta$  are given in degrees ( $360^\circ \equiv 2\pi$ ); UNDET for stands for “state undetermined”.  $SC_{L+P}^{\pi N, K\Lambda}$  for single-channel L+P fit to  $\pi N \rightarrow K\Lambda$ ,  $SC_{L+P}^{\gamma N, K\Lambda}$  for single-channel L+P fit to  $\gamma N \rightarrow K\Lambda$ ,  $CC_{L+P}^{\pi N, K\Lambda}$  for coupled-channel L+P fit to  $\pi N \rightarrow K\Lambda$  and  $\gamma N \rightarrow K\Lambda$ , etc. Under PDG, the PDG estimates are given or our own estimates from PDG entries.

	PDG	BnGa	$SC_{L+P}^{\pi N, K\Lambda}$	$SC_{L+P}^{\gamma N, K\Lambda}$	$CC_{L+P}$	PDG	BnGa	$SC_{L+P}^{\pi N, K\Lambda}$	$SC_{L+P}^{\gamma N, K\Lambda}$	$CC_{L+P}$
<b><math>N(1650)1/2^-</math></b>						<b><math>N(1710)1/2^+</math></b>				
$M_1$	1640-1670	1658±10	1667±43		1662±49	1670-1770	1690±15	1723±16		1697±23
$\Gamma_1$	100-170	102±8	75±16		59±16	80-380	155±25	37±14		84±34
$ a_1(\pi N \rightarrow K\Lambda) $	0.23±0.09	0.26±0.10	< 0.35		0.05±0.05	0.17±0.06	0.16±0.05	< 0.09		< 0.20
$\Theta_1(\pi N)$	(110±20)°	(110±20)°	(-123±237)°		(-95±33)°	(85±9)°	(-160±25)°	(-45±62)°		(-120±83)°
$10^3 \cdot  A_1(E_{0+}/M_{1-}) $		32±5			UNDET		32±16			UNDET
$\Theta_1(E_{0+}/M_{1-})$		(0±12)°			UNDET		(-40±30)°			UNDET
<b><math>N(1895)1/2^-</math></b>						<b><math>N(1880)1/2^+</math></b>				
$M_2$	1905±20	1895±15	1910±64	1901±18	1906±17	1870±40	1860±40	2081±293	1876±11	1878±11
$\Gamma_2$	100±40	132±30	119±24	68±18	100±11	220±50	230±50	48±183	31±9	33±9
$ a_1(\pi N \rightarrow K\Lambda) $	0.05±0.02	0.09±0.03	0.06±0.03		0.03±0.01	0.02±0.01	0.05±0.02	UNDET		0.15±0.05
$\Theta_2(\pi N \rightarrow K\Lambda)$	(-90±30)°	(8±30)°	(-77±107)°		(87±27)°	(32±10)°	(27±30)°	UNDET		(-82±9)°
$10^3 \cdot  A_2(E_{0+}/M_{1-}) $		22±17		30±21	51±25		18±12		8±6	8±5
$\Theta_2(E_{0+}/M_{1-})$		(-25±30)°		(-80±47)°	(-73±30)°		(90±70)°		(60±40)°	(59±40)°

**Table 3.** Pole parameters for the  $J^P = 3/2^+$ ,  $3/2^-$ , and  $5/2^-$  waves from the BnGa multichannel partial-wave analysis (BnGa). The  $E_{1+}$  and  $M_{1+}$  ( $E_{2-}$  and  $M_{2-}$ ) multipoles exciting the  $J^P = 3/2^+$  ( $3/2^-$ ) partial waves are fitted in a coupled multipole CM L+P fit, the  $E_{2+}$  in a single channel SC L+P fit. Masses and widths are given in MeV. The acronym  $|A_1(E_{1+}/E_{2-}/E_{2+})|$  stands for the residues  $|Res_1(E_{0+}(\gamma N \rightarrow K\Lambda))|$ ,  $|Res_1(E_{2-}(\gamma N \rightarrow K\Lambda))|$ , etc., which are given in  $\text{GeV}^{-1/2}$  units; the phases  $\Theta$  are given in degrees ( $360^\circ \equiv 2\pi$ ).  $CM_{L+P}^{\pi N, K\Lambda}$  denotes the coupled-multipole L+P fit to  $\gamma N \rightarrow K\Lambda$ ,  $SC_{L+P}^{\pi N, K\Lambda}$  the single-channel L+P fit to  $\gamma N \rightarrow K\Lambda$ . Under PDG, the PDG estimates are given or our own estimates from PDG entries.

	PDG	BnGa	$CM_{L+P}$	PDG	BnGa	$CM_{L+P}$	PDG	BnGa	$SC_{L+P}^{\gamma N, K\Lambda}$
<b><math>N(1900)3/2^+</math></b>				<b><math>N(1875)3/2^-</math></b>			<b><math>N(2060)5/2^-</math></b>		
$M_1$	1900-1940	1945±35	1912±30	1800-1950	1870±25	1977±41	2030-2130	2030±25	2019±51
$\Gamma_1$	130-300	135 $^{+70}_{-30}$	166±30	150-250	210±25	120±50	300-450	350 $^{+80}_{-30}$	141±67
$10^3 \cdot  A_1(E_{1+}/E_{2-}/E_{2+}) $		45±12			11±10			8±6	
$\Theta_1(E_{1+}/E_{2-}/E_{2+})$		(-100±20)°			(40±50)°			(-100±80)°	
$10^3 \cdot  A_1(M_{1+}/M_{2-})/M_{2+} $		80±30			9±8			60±18	
$\Theta_1(M_{1+}/M_{2-}/M_{2+})$		(95±30)°			(-30±100)°			(-170±10)°	

In a similar model, Skoupil and Bydžovský [62] use alternatively 15 or 16 resonances. They confirm the findings of the Gent group but report evidence that  $N(1880)1/2^+$  should be replaced by  $N(1860)5/2^+$ .

A number of groups have analyzed pion or photo-induced reactions with a Kaon and a  $\Lambda$  hyperon in the final state. Wu, Xie, and Chen [63] studied the reaction  $\pi^- p \rightarrow K^0\Lambda$  up to  $W = 1.76 \text{ GeV}$  in an isobar model; the isobars

include hyperon exchanges in the  $u$ -channel and  $K^*$  exchange in the  $t$ -channel. The leading  $s$ -channel contributions were found to be due  $N(1535)1/2^-$ ,  $N(1650)1/2^-$  and  $N(1720)3/2^+$  formation. Xiao, Ouyang, Wang, and Zhong [64] studied the mass range below 1.8 GeV and emphasize the leading role of  $N(1535)1/2^-$  and  $N(1650)1/2^-$ . The Jülich-Bonn (JüBo) group [58] described the data on  $\pi^- p \rightarrow K^0\Lambda$  simultaneously with other pion-induced re-



actions in an analytic, unitary, coupled-channel approach. SU(3) flavor symmetry was used to relate both the  $t$ - and the  $u$ -channel exchanges. The authors fit the available data (see Fig. 1); all resonances found in the GWU analysis [12] were introduced in the fit and four further ones.

Mart, Clympton and Arifi [65,66] take into account the set of resonances used in the BnGa analysis [15]. They find that spin-5/2 resonances play an important role and have to be taken into account. In their best fit, the authors use 17  $N^*$  resonances. The three resonances  $N(1650)1/2^-$ ,  $N(1720)3/2^+$ , and  $N(1900)3/2^+$  provide the most important contributions.

In Fig. 13, the photoproduction multipoles from the BnGa analysis and those of Skoupil and Bydžovský [62] and of Mart, Clympton and Arifi [65] are compared. There is no much similarity even though partly the same resonances are used. But possibly, this is not too surprising. In a comparison of the best studied process,  $\gamma p \rightarrow \pi N$ , significant differences were observed in the multipoles obtained by the BnGa, JüBo, and GWU groups [67] even though all three groups were capable of describing the data reasonably well. However, new data enforced a considerable reduction of the spread of the three results. In any case, the comparison demonstrates that further work is needed before the  $\gamma p \rightarrow K^+ \Lambda$  reaction can be considered as well understood.

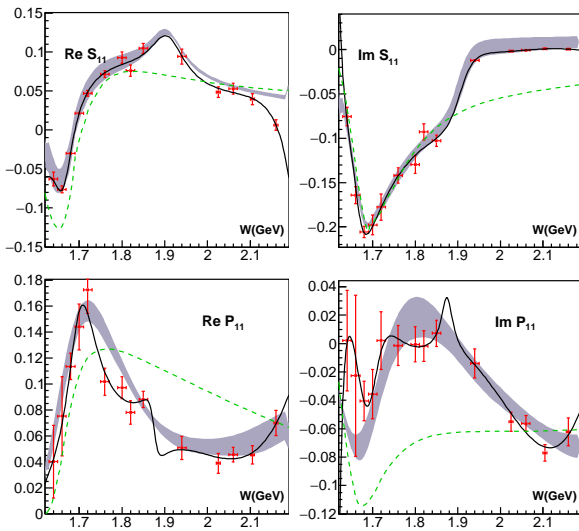


**Fig. 12.** Real and imaginary part of the (dimensionless)  $S_{11}$  and  $P_{11}$  waves [31]. The energy-dependent solution BnGa2011-02 is shown as error band. The solid curve represents a L+P fit. The dashed (green) curve is given by the solution JüBo2015-B of the JüBo group [58]. The BnGa and JüBo groups use a different sign convention. The JüBo amplitudes are shown with an inverted sign.

## 6 Summary

For a long time it has been anticipated that photoproduction experiments will provide measurements that are sufficient in number and statistical accuracy to construct the four complex amplitudes governing the photoproduction of an octet baryon and a pseudoscalar meson. A determination of these four amplitudes requires the measurement with sufficient accuracy of at least eight carefully selected observables [36], and one phase still remains undetermined. Alternatively, the multipoles driving the excitation of specific partial waves can be deduced from the data in a truncated partial wave analysis.

In this paper, we have performed such a truncated partial wave analysis of the reaction  $\gamma p \rightarrow K^+ \Lambda$ . The CLAS experiments studied this reaction and reported data on the differential cross section  $d\sigma/d\Omega$ , on the polarization observables  $P$ ,  $T$  and  $\Sigma$ , and on the spin correlation parameters  $O_x$ ,  $O_z$ ,  $C_x$ ,  $C_z$ . The data cover the resonance region from 1.71 to 2.13 GeV, mostly in 20 MeV wide bins. Thus at the moment, these data offer the best chance to perform a truncated partial wave analysis.

In a first step, we determined the number of multipoles that can be deduced from the data. When the number of free multipoles is increased in the energy-independent analysis, the errors in the determination of the multipoles increases, and one has to balance precision on the one hand and the number of multipoles on the other hand. It turned out that only the four largest multipoles,  $E_{0+}$ ,  $M_{1-}$ ,  $E_{1+}$ ,  $M_{1-}$ , can be determined without constraints when a good precision of the multipoles is required. In addition, three further multipoles,  $E_{2-}$ ,  $M_{2-}$ ,  $E_{1+}$ , could be derived from the data when a penalty function forced the fit not to deviate too much from an energy dependent solution. In addition to the photoproduction multipoles, we also used partial wave amplitudes for the reaction  $\pi^- p \rightarrow K^0 \Lambda$  which had been determined earlier.

The energy-dependent solution was found within the BnGa approach. In this approach, a large number of data on pion and photo-induced reaction is fitted in a coupled channel analysis. The data base includes  $N\pi$ ,  $N\eta$ ,  $\Delta K$ ,  $\Sigma K$ ,  $N\pi\pi$ , and  $N\pi\eta$  final states and, in an iterative procedure, the partial wave amplitudes and photoproduction multipoles derived here. The higher photoproduction multipoles that could not be determined in the fits to the CLAS data were kept fixed to multipoles from the BnGa analysis.

All multipoles considered here,  $E_{0+}$ ,  $M_{1-}$ ,  $E_{1+}$ ,  $M_{1+}$ ,  $E_{2-}$ ,  $M_{2-}$ ,  $E_{1+}$ , are fitted within a Laurent-Pietarinen expansion. This expansion exploits the analytic structure of the S-matrix. In the vicinity of a resonance position (and reasonably close to the real axis), the photoproduction amplitude is determined by poles and the opening of thresholds. When this analytic structure is imposed, fits to the photoproduction multipoles and partial wave amplitudes require no further dynamical input, the fits do not impose any model bias. The Laurent-Pietarinen fits were performed to the photoproduction multipoles, to the partial wave amplitudes from the  $\pi^- \rightarrow K^0 \Lambda$  reaction,

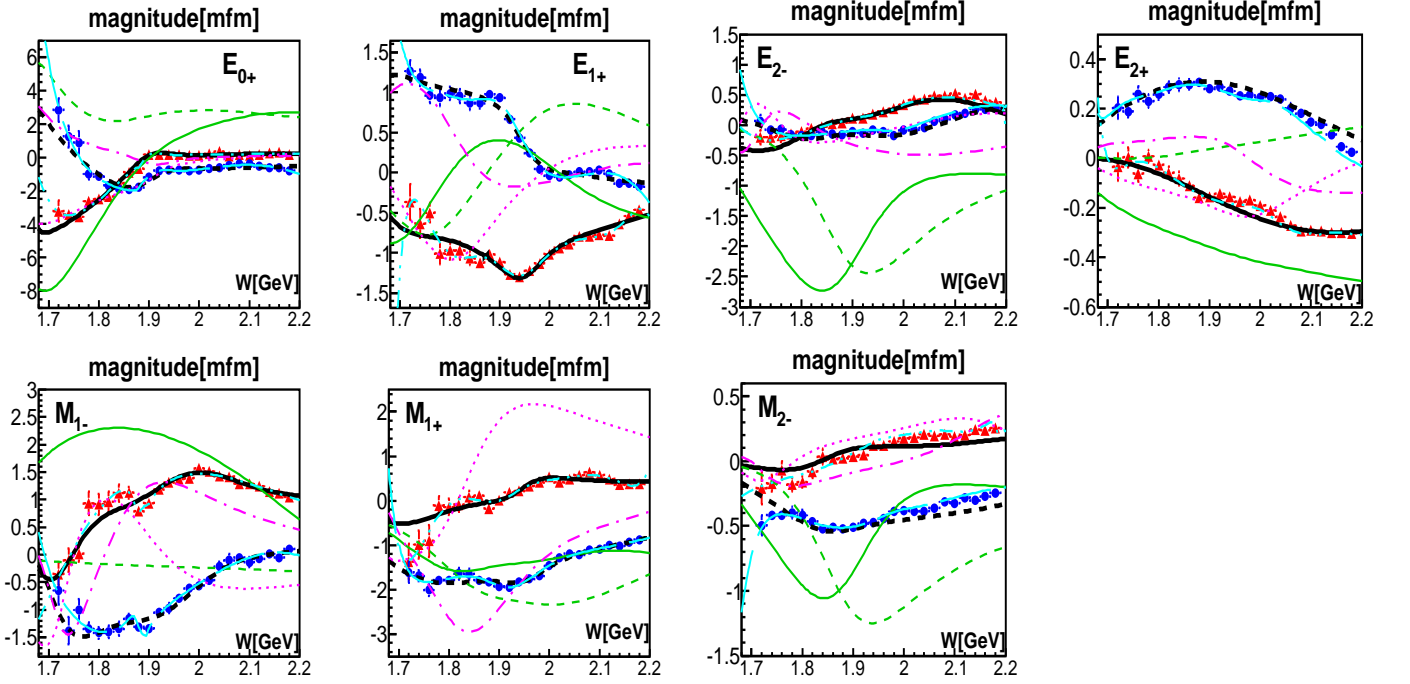


**Fig. 13.** (Color online) Comparison of the real and imaginary parts of the  $E_{0+}$ ,  $E_{1+}$ ,  $M_{1-}$ ,  $M_{1+}$ ,  $E_{2-}$ ,  $E_{2+}$ , and  $M_{2-}$  multipoles. The result of the energy-independent analysis is shown with error bars; the BnGa fit [15] to the real part is represented by (black) thick curves, to the imaginary part by thick dashed curves. The L+P fit, shown by (cyan) long-dashed and long-dashed-dotted curves, often coincides with the BnGa fit. The fit of Ref. [62] is shown by thin (green) solid or dashed curves, and the fit of Refs. [65, 66] by thin (magenta) dotted or dashed dotted curves, again for the real or imaginary parts, respectively. Refs. [65, 66] use a different sign convention. These amplitudes are shown with an inverted sign.

and to both in a coupled channel fit. The results are then compared to those from the BnGa fit.

The two resonances  $N(1895)1/2^-$  and  $N(1900)3/2^+$  are firmly established. The results on their masses, widths, and other properties agree well. Also the  $N(1880)1/2^+$  resonance is definitely required but there remains the question of the width: within the Laurent-Pietarinen expansion, its width is 40 MeV or less while its width within the BnGa approach is about 150 MeV. The statistical significance of the narrow width is however very small.

The two resonances  $N(1875)3/2^-$  and  $N(2060)5/2^-$  are derived from photoproduction multipoles which are constrained to follow the BnGa solution. In the  $J^P = 3/2^-$  partial wave, BnGa finds two poles; in the Laurent-Pietarinen fit, only one pole is observed at a mass in between the two BnGa poles. The BnGa and Laurent-Pietarinen results on  $N(2060)5/2^-$  are nicely consistent.

Summarizing, we can claim that several resonances found in the BnGa energy-dependent multichannel analysis are confirmed by fits based on a Laurent-Pietarinen expansion with a minimal model dependence.

This work is supported by the *Deutsche Forschungsgemeinschaft* (SFB/TR110), *Deutsche Forschungsgemeinschaft* (SFB 1014) the *US Department of Energy* under contract DE-AC05-06OR23177, the *U.K. Science and Technology Facilities Council* grant ST/L005719/1, and the *Russian Science Foundation* (RSF 16-12-10267).

## References

1. R. G. Edwards, J. J. Dudek, D. G. Richards and S. J. Wallace, *Phys. Rev. D* **84**, 074508 (2011).
2. S. Capstick and N. Isgur, *Phys. Rev. D* **34**, 2809 (1986).
3. M. Ferraris, M. M. Giannini, M. Pizzo, E. Santopinto and L. Tiator, *Phys. Lett. B* **364**, 231 (1995).
4. L. Y. Glozman, W. Plessas, K. Varga and R. F. Wagenbrunn, *Phys. Rev. D* **58**, 094030 (1998).
5. U. Löring, B. C. Metsch and H. R. Petry, *Eur. Phys. J. A* **10**, 395 (2001).
6. M. M. Giannini and E. Santopinto, *Chin. J. Phys.* **53**, 020301 (2015).
7. C. Patrignani *et al.* [Particle Data Group], *Chin. Phys. C* **40**, no. 10, 100001 (2016).
8. R. Koniuk and N. Isgur, *Phys. Rev. Lett.* **44**, 845 (1980).
9. R. Koniuk and N. Isgur, *Phys. Rev. D* **21**, 1868 (1980) Erratum: [*Phys. Rev. D* **23**, 818 (1981)].
10. G. Höhler, *Pion Nucleon Scattering. Part 2: Methods And Results and Phenomenology*, edited by G. Höhler and H. Schopper (Springer, 1983) 601 P.
11. R. E. Cutkosky, C. P. Forsyth, J. B. Babcock, R. L. Kelly and R. E. Hendrick, “Pion - Nucleon Partial Wave Analysis,” 4th Int. Conf. on Baryon Resonances, Toronto, Canada, Jul 14-16, 1980 (Toronto University Press, 1980) p.19 (QCD161:C45:1980).
12. R. A. Arndt, W. J. Briscoe, I. I. Strakovsky and R. L. Workman, *Phys. Rev. C* **74**, 045205 (2006).
13. S. Capstick and W. Roberts, *Phys. Rev. D* **58**, 074011 (1998).

14. S. Capstick and W. Roberts, Prog. Part. Nucl. Phys. **45**, S241 (2000).
15. A.V. Anisovich, R. Beck, E. Klempt, V.A. Nikonov, A.V. Sarantsev and U. Thoma, Eur. Phys. J. A **48**, 15 (2012).
16. D. M. Manley and E. M. Saleski, Phys. Rev. D **45**, 4002 (1992).
17. G. Penner and U. Mosel, Phys. Rev. C **66**, 055211 (2002).
18. G. Penner and U. Mosel, Phys. Rev. C **66**, 055212 (2002).
19. M. Shrestha and D. M. M. Manley, Phys. Rev. C **86**, 045204 (2012).
20. M. Shrestha and D. M. Manley, Phys. Rev. C **86**, 055203 (2012).
21. A. Švarc, M. Hadžimehmedović, R. Omerović, H. Osmanović, and J. Stahov, Phys. Rev. **C89**, 45205 (2014).
22. A. Anisovich, E. Klempt, A. Sarantsev and U. Thoma, Eur. Phys. J. A **24**, 111 (2005).
23. A.V. Anisovich and A.V. Sarantsev, Eur. Phys. J. A **30**, 427 (2006).
24. A.V. Anisovich, V.V. Anisovich, E. Klempt, V.A. Nikonov and A.V. Sarantsev, Eur. Phys. J. A **34**, 129 (2007).
25. I. Denisenko *et al.*, Phys. Lett. B **755**, 97 (2016).
26. V. A. Nikonov, A. V. Anisovich, E. Klempt, A. V. Sarantsev and U. Thoma, Phys. Lett. B **662**, 245 (2008).
27. T. M. Knael *et al.*, Phys. Rev. D **11**, 1 (1975).
28. R. D. Baker *et al.*, Nucl. Phys. B **141**, 29 (1978).
29. D. H. Saxon *et al.*, Nucl. Phys. B **162**, 522 (1980).
30. K. W. Bell *et al.*, Nucl. Phys. B **222**, 389 (1983).
31. A. V. Anisovich *et al.*, Eur. Phys. J. A **50**, 129 (2014).
32. G. F. Chew, M. L. Goldberger, F. E. Low and Y. Nambu, Phys. Rev. **106**, 1345 (1957).
33. I. S. Barker, A. Donnachie and J. K. Storrow, Nucl. Phys. B **95**, 347 (1975).
34. C. G. Fasano, F. Tabakin and B. Saghai, Phys. Rev. C **46**, 2430 (1992).
35. G. Keaton and R. Workman, Phys. Rev. C **54**, 1437 (1996).
36. W. T. Chiang and F. Tabakin, Phys. Rev. C **55**, 2054 (1997).
37. A. M. Sandorfi, S. Hoblit, H. Kamano and T.-S. H. Lee, J. Phys. G **38**, 053001 (2011).
38. Y. Wunderlich, F. Afzal, A. Thiel and R. Beck, arXiv:1611.01031 [physics.data-an].
39. Y. Wunderlich, R. Beck and L. Tiator, Phys. Rev. C **89**, no. 5, 055203 (2014).
40. R. Bradford *et al.* [CLAS Collaboration], Phys. Rev. C **73**, 035202 (2006).
41. M. E. McCracken *et al.* [CLAS Collaboration], Phys. Rev. C **81**, 025201 (2010).
42. R. K. Bradford *et al.* [CLAS Collaboration], Phys. Rev. C **75**, 035205 (2007).
43. C. A. Paterson *et al.* [CLAS Collaboration], Phys. Rev. C **93**, no. 6, 065201 (2016).
44. S. U. Chung, J. Brose, R. Hackmann, E. Klempt, S. Spanier and C. Strassburger, Annalen Phys. **4**, 404 (1995).
45. R. L. Workman, L. Tiator and A. Sarantsev, Phys. Rev. C **87**, no. 6, 068201 (2013).
46. A. V. Anisovich, E. Klempt, V. A. Nikonov, A. V. Sarantsev and U. Thoma, Eur. Phys. J. A **49**, 158 (2013).
47. V. Sokhoyan *et al.* [CBELSA/TAPS Collaboration], Eur. Phys. J. A **51**, no. 8, 95 (2015) Erratum: [Eur. Phys. J. A **51**, no. 12, 187 (2015)].
48. E. Gutz *et al.* [CBELSA/TAPS Collaboration], Eur. Phys. J. A **50**, 74 (2014).
49. A. Švarc, M. Hadžimehmedović, H. Osmanović, J. Stahov, L. Tiator, and R. L. Workman, Phys. Rev. **C88**, 035206 (2013).
50. Michiel Hazewinkel: *Encyclopaedia of Mathematics*, Vol.6, Springer, 31. 8. 1990, p. 251.
51. S. Ciulli and J. Fischer in Nucl. Phys. **24**, 465 (1961).
52. I. Ciulli, S. Ciulli, and J. Fisher, Nuovo Cimento **23**, 1129 (1962).
53. E. Pietarinen, Nuovo Cimento Soc. Ital. Fis. **12A**, 522 (1972).
54. E. Pietarinen, Nucl. Phys. **B107**, 21 (1976).
55. A. Švarc, M. Hadžimehmedović, H. Osmanović, J. Stahov, L. Tiator, and R. L. Workman, Phys. Rev. **C89**, 065208 (2014).
56. A. Švarc, M. Hadžimehmedović, H. Osmanović, J. Stahov, and R. L. Workman, Phys. Rev. **C91**, 015207 (2015).
57. A. Švarc, M. Hadžimehmedović, H. Osmanović, J. Stahov, L. Tiator, R. L. Workman, Phys. Lett. **B755**, 452 (2016).
58. D. Rönchen *et al.*, Eur. Phys. J. A **51**, no. 6, 70 (2015).
59. V. L. Kashevarov *et al.* [A2 Collaboration], Phys. Rev. Lett. **118**, no. 21, 212001 (2017).
60. L. De Cruz, T. Vrancx, P. Vancraeyveld and J. Ryckebusch, Phys. Rev. Lett. **108**, 182002 (2012).
61. L. De Cruz, J. Ryckebusch, T. Vrancx and P. Vancraeyveld, Phys. Rev. C **86**, 015212 (2012).
62. D. Skoupil and P. Bydžovský, Phys. Rev. C **93**, no. 2, 025204 (2016).
63. C. Z. Wu, Q. F. L, J. J. Xie and X. R. Chen, Commun. Theor. Phys. **63**, no. 2, 215 (2015).
64. L. Y. Xiao, F. Ouyang, K. L. Wang and X. H. Zhong, Phys. Rev. C **94**, no. 3, 035202 (2016).
65. T. Mart, S. Clymton and A. J. Arifi, Phys. Rev. D **92**, no. 9, 094019 (2015).
66. T. Mart and S. Sakinah, Phys. Rev. C **95**, no. 4, 045205 (2017).
67. A. V. Anisovich *et al.*, Eur. Phys. J. A **52**, no. 9, 284 (2016).